Assessment of Various Thermoplastic Masks Used for Radiation Therapy Immobilization in Terms of Shrinkage and Pressure

Written by:

Ayman Sameer Tunkr, B.Sc. Medical Physics

A Thesis Submitted in Partial Fulfillment of the Requirements of the Degree of Master of Science

McMaster University

Department of Medical Physics and Applied Radiation Science

March 10, 2014

Assessment of Various Thermoplastic Masks Used for Radiation Therapy Immobilization in Terms of Shrinkage and Pressure

Written by:

Ayman Sameer Tunkr, B.Sc. Medical Physics

Supervised by

Orest Ostapiak, Ph.D., FCCPM

This work has been performed at Department of Medical Physics
Juravinski Cancer Center, ON, Hamilton, Canada
March 10, 2014

McMaster University

Department of Medical Physics and Applied Radiation Sciences

Abstract

The aims of this study are first, to assess and compare the amount of deformation for seven thermoplastic masks from three different manufacturers [Aquaplast RT-1889YS (Aqua variable perf), Fiberplast RT-1889KYS (Fiber variable perf), Embrace RT-8320 (Embrace), AccuPerf IMRT head mask RG461-4SHT (AccuPerf), Fiberplast RT-1889KS (Fiberplast), Aquaplast RT-1989S (Aqua thick), and Aquaplast RT-1889S(Aquaplast)] using time lapse photography, and second, to measure the amount of pressure exerted by each mask on a rigid head phantom using pressure sensitive film.

For the first aim, all masks were marked with fiducial points located near forehead, nose, and chin. The masks were fabricated on a rigid head phantom following manufacturer instructions. Each mask was mounted on a plastic mounting tray, and photographed in a sagittal view over the span of one week. The fiducial coordinates were determined by a center of mass algorithm. A scale factor was determined by photographing a graph sheet mounted in place of the mask.

For the second aim, the pressure exerted by each mask was evaluated by mounting the mask on the head phantom after sandwiching a strip of pressure sensitive film between the two at three anatomical locations: the forehead, nose, and chin.

Measurement of translation in the posterior direction did not give reproducible results as direct caliper measurements did not agree with those from the time-lapse photography technique.

In the superior/inferior direction, the Embrace mask showed the greatest deformation at forehead and nose areas (1.069±0.017mm (inferiorly), and 0.432±0.010mm (inferiorly) respectively), while the Aqua thick mask showed the greatest deformation at chin area (0.970±0.016mm (superiorly)).

The averaged median pressure of the masks at the forehead location were not significantly different except for the Fiber variable perf which showed the greatest averaged median pressure (0.118 MPa). At the nose location, no mask showed a significantly different averaged median pressure. At the chin location, the Aqua thick mask showed a significantly higher averaged median pressure compared to the others (0.180 MPa).

Acknowledgment

All praises and thanks are due to Allah (God) Who has created me from nothing, “Has there [not] come upon man a period of time when he was not a thing [even] mentioned?” The Holey Quran chapter 76. And peace and blessing of Allah be upon our prophet Mohammad son of Abduallah “peace be upon him” who has been sent as a messenger for mankind (people and devil) to convey the message of Allah “Our Lord, and send among them a messenger from themselves who will recite to them Your verses and teach them the Book and wisdom and purify them. Indeed, You are the Exalted in Might, the Wise." The Holey Quran chapter 2.

I love to thank my parents who have brought me up from childhood and their endless kindness to me, “And lower to them (parents) the wing of humility out of mercy and say, "My Lord, have mercy upon them (parents) as they brought me up [when I was] small." The Holey Quran chapter 17.

Many thanks for my wife who has been patient with me, and inner support in my life.

Ultimately, I would like to appreciate my supervisor, Dr. Orest Ostapiak, and thesis committee, Dr. Kevin Diamond, and Dr. Joseph Hayward who have been helpful for progressing this study with firm patience and full intelligence. Also I would like to thank the workshop, Bud Thomas and Randy Passow and mould room staff, Greg Saweski for their support.

I would like to acknowledge Ron Wallace of Harpell and Associates for supplying some of the mask samples.

Table of Contents

Table of Figures

Table of Tables

1. CHAPTER 1: INTRODUCTION

1.1. Introduction to thermoplastic material

Thermoplastics are organic materials which soften when they are heated. They can be formed after softening and retain their final shape when cooled. In terms of properties, the chemistry of thermoplastics is similar to rubber, while the strength is similar to aluminum. They are light in weight with densities of 0.9 to 2 gm/cc. These properties along with low cost make them appropriate for various applications(“What Are Thermoplastics?,” 2007).

1.2. Significance of thermoplastic masks in the radiation-therapy treatment

The essential aim of radiation therapy is to deliver a specified dose to a target volume accurately while protecting healthy tissues and significant structures (Sweeney et al., 1998). This accuracy requires that the error in total dose be within ±5%, as recommended by the International Commission of Radiation Units (ICRU). In addition, to take uncertainty of patient positioning and alignment of the treated radiotherapy beams during treatment and for entire treatment course into consideration, a set-up margin for each beam is necessary (*ICRU 62*, 1999). The size of the set-up margin relies on the selection of beam geometries which can be different from one anatomical site to another (*ICRU 62*, 1999). The set-up margin is affected by the following factors: variations in patient positioning , mechanical uncertainty of the equipment, dosimetric uncertainties, transfer set-up errors from CT and simulator to the treatment unit, human factors (*ICRU 62*, 1999). These factors may differ from center to center (*ICRU 62*, 1999). The set-up margin also is affected by the positioning reproducibly of the treated part of a patient’s body, i.e. if a tumor is located in a patient’s brain, then the set-up margin is generally smaller than that of a tumor located in a patient’s lung which must account for breathing motion (*ICRU 62*, 1999). The set-up margin is used at the Juravinski cancer center physicist is 3-

5mm for head and neck tumors. Therefore, radiation-therapy treatment for patients, especially, those with brain, or head and neck cancers requires a reproducible setup throughout the entire treatment course. Otherwise, critical structures adjacent to targets may be irradiated unnecessarily (Gilbeau et al., 2001). Thus, treatments that involve conformal radiotherapy or intensity-modulated radiotherapy, which are used to treat sites in the head and neck by delivering a fractionated dose , typically use an immobilization device known as a thermoplastic mask to immobilize the patient's head and neck during the treatment course (Sharp et al., 2005). These thermoplastic masks must be simple to use , and balance patient comfort against rigidity(Fuss et al., 2004).

A thermoplastic mask can be formed easily on a patient after being softened by immersion in a 37^{0}C water bath. The thermoplastic mask is then reshaped on a patient and allowed to cool, becoming hard in about 5-10 minutes. It is then kept at room temperature until the first radiation therapy treatment for the patient, which may be a few days or weeks later. Therefore, the mask should fit on the patient as well then as the moment after formation (Bogdanov, 2003).

One study investigated the setup accuracy of three different thermoplastic masks (Posicast®): head mask with three fixation points, head and shoulder mask with four fixation points, and head and shoulder mask with five fixation points. These thermoplastic masks are uniformly perforated and manufactured without Kevlar fiber(but thickness was not reported). 30 patients were assigned randomly to these masks and all patients underwent treatment simulation. For patients who had head and neck tumors, three fictitious isocenters were positioned (one at neck level, one at shoulder level and one at head level). Patients were positioned using the projections of laser beams onto orthogonal markers placed on the thermoplastic masks. Successive Portal as well as simulator images were obtained for comparison. The amount of displacement between the simulator and successive portal images was computed. 915 portal images were acquired, and 98% of them were analysed. Over all masks, the displacement had a standard deviation of 2.2 mm from the mean value at the level of the head and neck in the medio-lateral direction; whereas, at the shoulder level, the total displacement had a standard deviation of 2.8mm from the mean value in the medio-lateral and cranio-caudal directions. They concluded that a thermoplastic mask is sufficient for the immobilizing head, neck and shoulders of a patient (Gilbeau et al., 2001).

Another study was performed to assess the repositioning accuracy of three commercial thermoplastic masks of type Efficast®/Pelvicast™ Raycast©-HP mask system (Orfit Industries, Wijnegem, Belgium). There were no specifications mentioned about these masks in terms of perforation pattern, material composition or thickness but they were pre-cut masks. The experiment involved twenty-two patients who underwent repeated CT images during their treatment. The masks were marked with multiple anatomical landmarks which were used to assess the shift of the landmarks coordinates using a CT scan. The translation of the target isocenters of the landmarks in x, y and z components from the initial set up was calculated using an iterative optimization algorithm. The translation of the mean target isocenter was 0.74mm in the x direction, 0.75mm in the y direction, and 0.93mm in the z direction, concluding that the Orfit thermoplastic masks are more accurate than other thermoplastic masks. (Fuss et al., 2004).

A review study assessed the reproducibility of the thermoplastic mask system throughout the entire radiation treatment. Anatomic points were marked on orthogonal radiographs and digitized by performing a three-dimensional analysis for nine patients. The result showed that the total movement in three directions of patient position can be limited to 2mm (Thornton et al., 1991).

1.2.1. Variations in thermoplastic mask styles from different manufactures

Manufacturers produce a variety of head and neck thermoplastic masks with different perforation patterns, material compositions, and thicknesses. Masks are available with regular perforations distributed throughout the mask or with various perforation patterns. Perforation density may vary from 40% to 20%. Thermoplastic material is the main constituent of a thermoplastic mask. Some thermoplastics incorporate Kevlar fiber. Masks are available in four different thicknesses 1.6, 2.4, 3.2, and 4.8 mm.

1.2.2. Advantages and disadvantages of the various styles

There are pros and cons to using different styles of thermoplastic masks in terms of post-fabrication shrinkage, patient comfort, strength, and stiffness.

The manufacturer of Q-fix claims that there is a proportional relationship between amount of post-fabrication shrinkage and the perforation density. Also there is an inverse relationship between the strength of a mask and the perforation density (Q-fix, 2013). If the mask is perforated uniformly with either 40 or 20 percent perforations, then the mask will have low rigidity, uniform shrinkage, and feel uncomfortable to a patient (Q-fix, 2013). On the other hand, if the mask is made with solid areas along certain directions (non-uniform perforation), then the mask will have greater strength, reduced shrinkage, and feel more comfortable to a patient (Q-fix, 2013).

Moreover, the Q-fix manufacturer claims that the material composition of a mask can affect its rigidity and shrinkage. Aquaplast masks shrink more and are less rigid than Fiberplast masks which incorporate Kevlar fiber to increase mask stiffness and decrease shrinkage for improved patient comfort (Q-fix, 2013).

The thickness of the thermoplastic mask also influences stiffness and the amount of shrinkage; whereby a thicker mask is more rigid, but shrinks more.

1.3. Previous studies assessing the amount of shrinkage for various thermoplastic masks styles

A study was performed to measure the shrinkage force of three thermoplastic masks (UONTH from Orfit Industries, Uni-frameTH from Med-Tec, and U-frameTH from WFR). The shrinkage of the masks is due to its material crystallization. Masks were made from thermoplastic material, had a non-uniform perforation pattern, but no thickness was specified. The internal shrinkage force was tested using Lloyd Instruments Materials Testing machine (LRX Plus) which was used to measure the shrinkage force of a material by inserting a sample of thermoplastic between the grips of the machine after being moulded, and then stretched by about 50%. Subsequently, shrinkage force for that sample was recorded as a function of time. The internal shrinkage force for the thermoplastic mask material sample increased for 24 hours, then held relatively constant until 170 hours as shown in Figure 1 (Bogdanov, 2003).

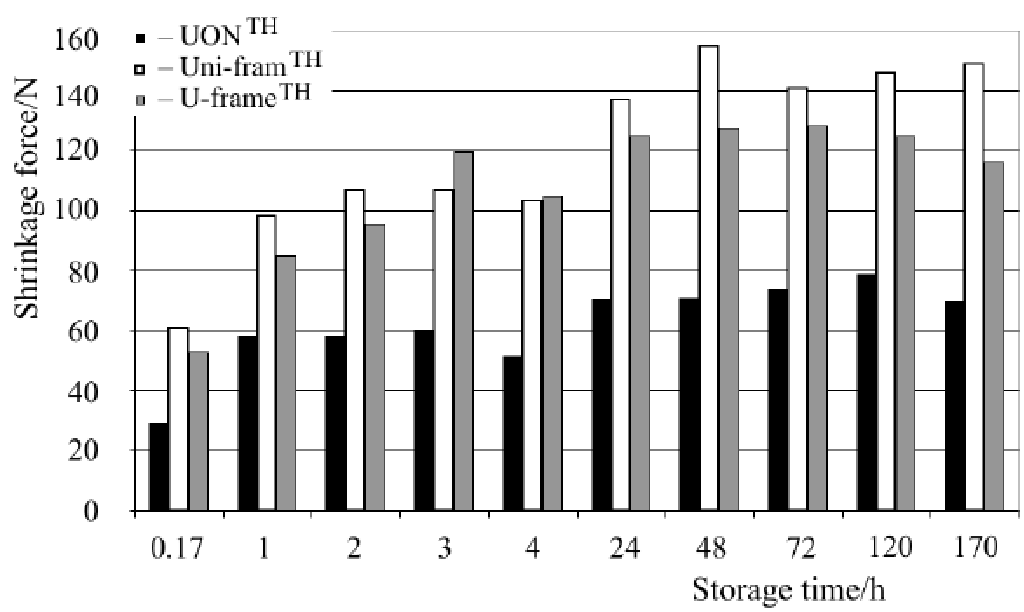

Figure 1. The internal shrinkage force for three thermoplastic masks (UONTH, Uni-frameTH and U-frameTH) over time (Bogdanov, 2003)**.**

Another study investigated the amount of shrinkage for four thermoplastic masks from one manufacturer, which were either Aquaplast or Fiberplast, which contain a Kevlar® fiber. The perforation pattern of the masks were either standard perforation pattern or variable perf perforation pattern called Variable Perf™. The amount of shrinkage was assessed by scanning the masks, which were marked with 1mm radio-opaque fiducial points located at nine different locations, using a CT scanner. The CT scan for each mask was obtained at one and a half hours, one week, two weeks, and three weeks post fabrication. The results showed that the total mean shrinkage for the standard perforation pattern thermoplastic masks was remarkably different from that of corresponding variable Perf ™ masks which underwent a greater amount of shrinkage (Dovell et al., 2014) contrary to manufacturer claims

Another study assessed the amount of shrinkage for an AccuPerf IMRT head mask, Klarity Green RG461-4SHT. The mask was heated in a 71^{0}C water bath and reshaped on a head phantom to dry. After hardening, the mask was measured with a caliper. After 24 hours the mask was again measured. The difference between the two dimensions was used to determine that the percentage of shrinkage was 6% (Rohrer).

One method used at the Juravinski cancer center to deal with the consequences of shrinkage is to place a spacer of thickness 3mm under the head rest for patients. This spacer is used during thermoplastic mask fabrication. The main purpose of the spacer is to accommodate shrinkage. The spacer is inserted under the patient's head rest flange to shift the patient's head in the anterior direction. After the mask shrinks, the spacer is removed. Figure 2 illustrates the use of the spacer to relieve pressure of the mask on the patient after the mask shrinks.

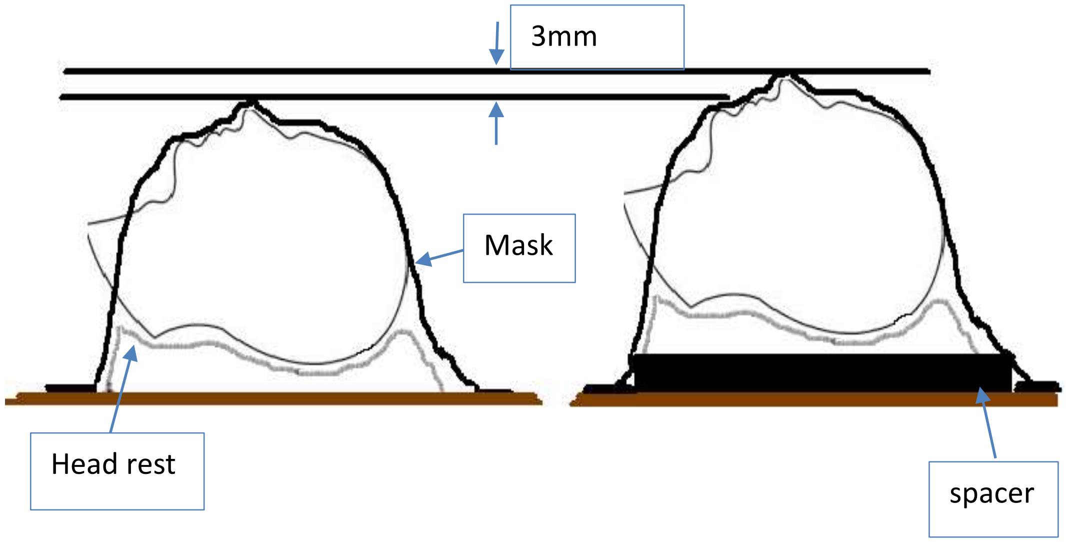

Figure 2. The head phantom with and without the spacer. Not drawn to scale

Hence, in order for head and neck thermoplastic masks to be effective in radiation therapy treatment, mask shrinkage has to be taken into consideration before the beginning of a treatment.

1.4. Study objectives

The first aim of this study is to assess and compare the total amount of unconstrained deformation/shrinkage for seven different thermoplastic masks styles from three different manufactures using a time-lapse photography technique whereby fiducial points marked along the anterior sagittal profile of the masks near forehead, nose, and chin are observed.

The following table sets out information about the masks evaluated.

Image of the mask	Mask reference name	Mask model number and manufacturer	description	Thickness mm
	Aqua variable perf	Aquaplast RT-1889YS Q-fix	Aquaplast thermoplastic mask	3.2
	Fiber variable perf	Fiberplast RT-1889KYS Q-fix	Fiberplast thermoplastic mask with Kevlar	3.2
	Fiberplast	Fiberplast RT-1889KS Q-fix	Fiberplast thermoplastic mask with Kevlar	3.2
	Aquaplast	Aquaplast RT-1889S Q-fix	Aquaplast thermoplastic mask	3.2

	Aqua thick	Aquaplast RT-1989S0 Q-fix	Aquaplast thermoplastic mask	4.8
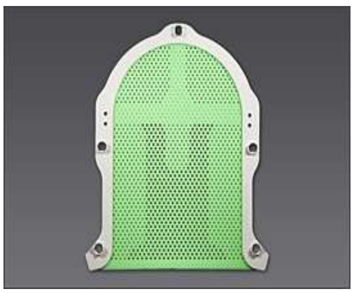	AccuPerf	AccuPerf IMRT head mask RG461-4SHT Klarity green mask	Low shrinkage and non-stick proprietary material	3.2
	Embrace	Embrace RT-8320 Bionix	Premium low-melt material with even hole distribution pattern after molding	3.2

Table 1. Information about the seven thermoplastic masks. The first and last two masks are non-uniform perforated.

The second objective is to measure the pressure exerted by the masks on the rigid head phantom on which they were formed at specific anatomical locations using pressure sensitive film. The film consists of two sheets: one coated with a developer and the other coated with microcapsules that break, introducing a red color. The amount of pressure is therefore proportional to the density of the red pixels: the more pressure that is applied the greater the density of red pixels.

2. <u>CHAPTER 2: Methodology</u>

2.1. Experimental method of unconstrained deformation assessment

2.1.1. Method of preparing the masks:

2.1.1.1. Marking the masks with fiducial points:

All masks were marked with fiducial points located along the masks near the head, nose and chin (Figure 3). These points were used to observe the deformation of the masks over a span of a week using a camera. Images were acquired at 5 minutes, 6 minutes, 1 hour, 2 hours, 3, hours, 4 hours, 24 hours, 48 hours, 72 hours, 96 hours, 120 hours, 144 hours, 168 hours and 192 hours.

Figure 3.The fiducial points marked along the mask.

2.1.1.2. Mask formation

Although, the masks were from different manufacturers, the procedure for formation was identical for each. A hot water bath at a temperature of 65^{o} C was used. The mask was immersed in the water bath for about 1 minute until the material of the mask softened. After the removal of the mask from the water bath, it was shaken to remove excess water and then pre-stretched about 15 cm by hand. Afterward, the mask was reshaped onto a rigid anthropomorphic head phantom on a Silverman head-rest and clamped on a specially adopted plastic mounting tray by its base-frame using swivel clamps and bolt and allowed to harden for about 15 minutes. During that time, the mask was shaped with fingers to conform to the head phantom. During the time of cooling, the first image was obtained which corresponded to time 0 hour image. The mask was then removed after 15 minutes from the head phantom and remounted on the same plastic mounting tray.

2.1.1.3. The plastic mounting tray criteria

Since all the masks were fabricated in sequence, a plastic mounting tray was designed for each mask to allow precise relocation of the mounted mask for imaging. The design criteria for the plastic mounting tray were: two perpendicular machined sides for accurate registration against corresponding perpendicular fences, and threaded holes to accept mounting bolts and swivel clamps at appropriate locations along the mask frame base. In addition, precision machined pins located on the left and right sides of the plastic mounting tray were used to reposition the mask precisely to the same position on the plastic mounting tray when the mask was removed to allow removal of the head phantom. The error of repositioning the mask on the plastic mounting tray was estimated to be 0.1mm. Two orthogonal fences clamped to an optical bench, were used for reproducibly registering the straight-edge of the plastic mounting tray (Figure 4).

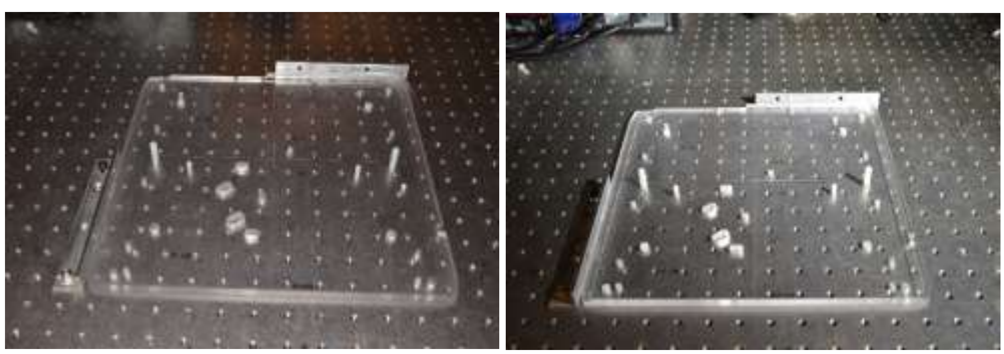

Figure 4. The plastic mounting tray registered with fences.

2.1.2. Mask photography

A DSLR Nikon D7000 camera fitted with a Nikon AF Nikkor 50 mm prime lens was mounted on a steady base (Figure 5) on the optical bench and connected to a laptop computer running software in order to acquire the time-lapse photographs.

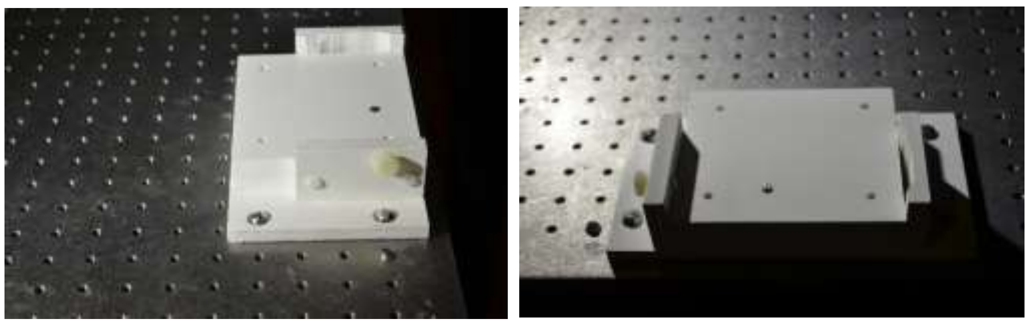

Figure 5. Camera base.

The specifications of the camera are as follows:

Specification	Details
Sensor size	23.6 x 15.6 mm CMOS
Effective pixels	16.2 million.
File format	NEF(RAW): 12 or 14 bit format, and JPEG format
Shutter speed	From 1/8000 s to 30 s
ISO range	From 100 to 6400, H1, and H2 equivalent to 12800, and 25600 respectively.

Table 2. Camera specification(Nikon, 2014)**.**

The lens features negligible pincushion and barrel distortion. This lens has a maximum aperture of f/1.8.

Three variables that affect the quality of the final image are: aperture; shutter speed; and ISO of the camera. The three variables are explained below:

Aperture or f/stop is the diaphragm in the lens itself or subsequent to the lens which controls the amount of light passing through the lens. Furthermore, it plays a key role in determining the depth of focus of an image. If the diaphragm is adjusted to have a wide diameter (small f/stop), then more light passes through the lens to the camera sensor (Figure 6)(Sony).

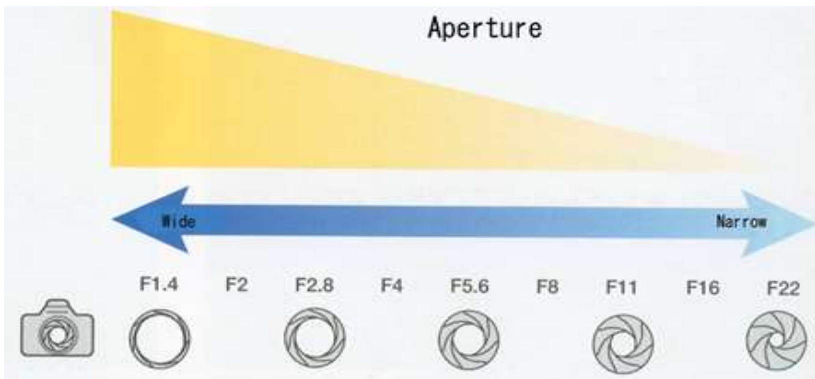

Figure 6. Illustration of the diaphragm in the lens (Aperture) (Sony)**.**

Shutter speed controls the length of time the camera shutter remains opened. It must be chosen so that subject motion is negligible during the exposure. If the shutter speed is set to 1/8000s (short shutter speed), then less light will enter to the camera sensor. (Figure 7)(Sony).

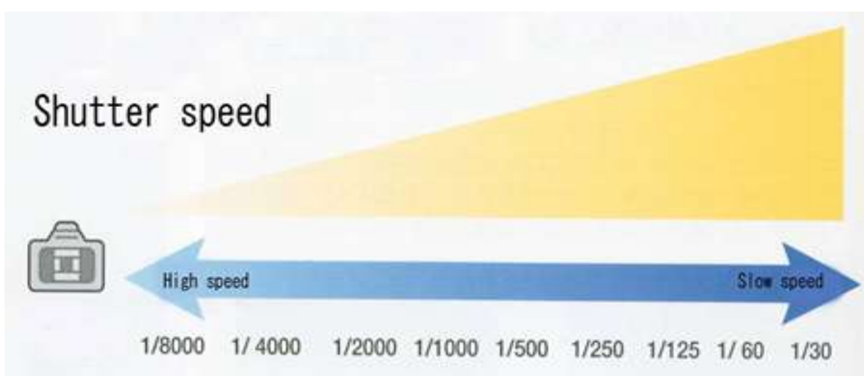

Figure 7. Illustration of the shutter speed adjustment (Sony)**.**

ISO stands for “International Standards Organization”. ISO refers to the sensitivity of the camera sensor to light, and it affects the amount of noise presented in the image. The more light illuminating the subject during the exposure, the lower the ISO setting required for correct exposure (Sony).

Figure 8 illustrates the relationship among the three variables and the depth of field, motion of the object, and the noise.

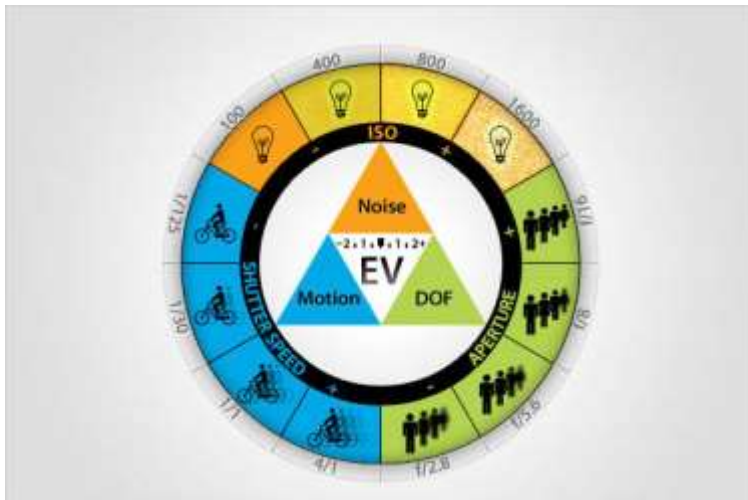

Figure 8. The relationship between aperture, shutter speed and ISO and with depth of field, motion, and noise respectively (Zhang, 2012)**.**

The relationship among the three variables can be defined as follows: a smaller f/stop (wide aperture), allows a faster shutter speed, or lower ISO value for correct exposure, while a higher f/stop (small aperture), requires a slower shutter speed, or a higher ISO value for the same correct exposure (Miller).

On the other hand, the relationship between the aperture, the shutter speed, and the ISO with the depth of field, motion, and noise respectively can be defined as follows: there is an inverse relationship between the aperture and the depth of field. If the aperture is adjusted to have a wide diaphragm or small f/stop, then the image will have a shallow depth of field. But, if the aperture is adjusted to have a small diaphragm or a high f/stop, then the image will have a deep-depth-of-field (Miller).

The relationship between the shutter speed and the motion of the object is also inverse. If a fast shutter speed is selected, blur due to the motion of the object will be reduced (Figure 8).

Ultimately, the noise in an image is determined by the value of ISO selected, the higher ISO, the more noise will be present (Miller).

In order to balance the trade-offs in imaging parameters, the aperture was adjusted to f/13, the shutter speed was adjusted to one tenth of a second (1/10 s), and since a LED light bulb, equivalent to 90 watt of a normal light bulb illuminated the masks during imaging, the ISO was adjusted to 100 which yields a relatively noise-free image.

The following table will illustrate other input commands to the camera:

Command's name	Selection
Focus	Manual focus with a single point
White balance	Auto white balance
Picture control	Monochrome
Image format	JPG Fine

Table 3. Other input commands to the camera.

Figure 9 The geometry for the unconstrained mask experiment:

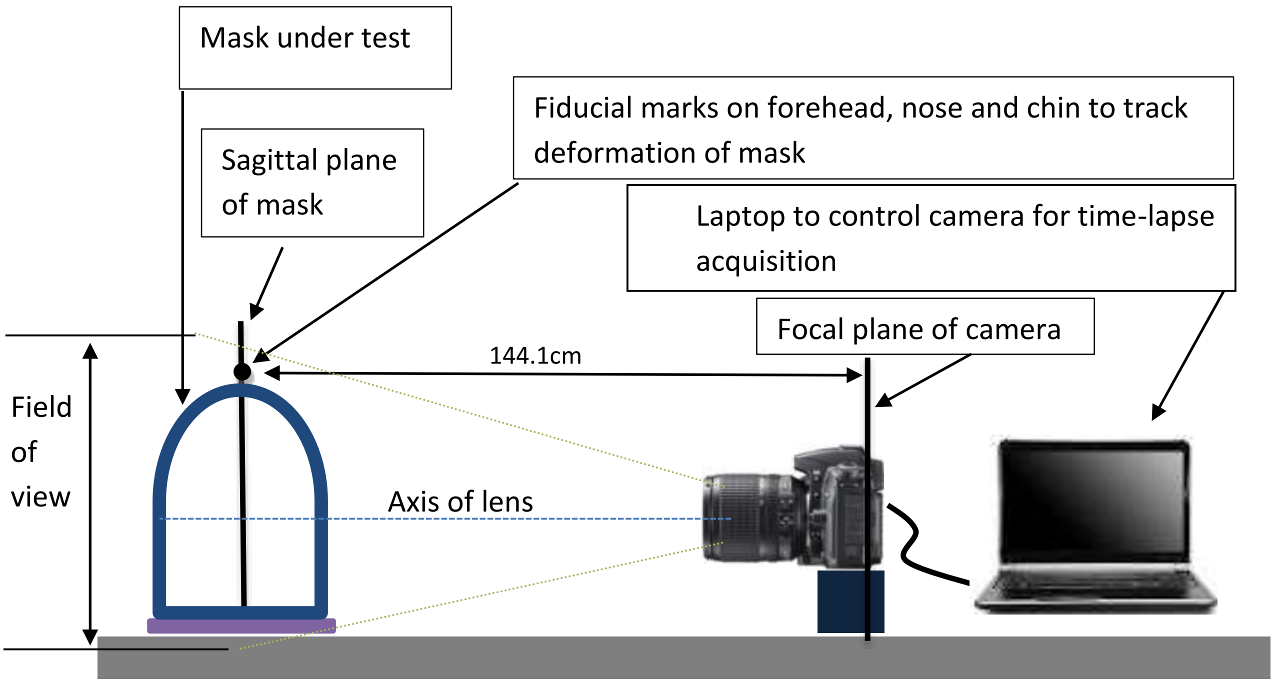

Figure 9. Geometry setup

The lens axis of the camera was perpendicular to the sagittal plane of the mask. This plane was placed 144.1cm from the focal plane of the camera. This resulted in a field of view of ≈ 46cm.

2.1.2.4. pixel position determination

The camera was connected to a laptop through a USB connector, and controlled using time-lapse software (digiCamControl) (Joergensen, 2012). The software was configured to capture a sequence of images for the mask. The images then were analysed by tracking the three fiducial marks on each mask. The pixel coordinates of each fiducial were determined using a center of mass algorithm within an image processing software program called ImageJ (Rasband). The center of mass algorithm determines the inverse grey-value weighted position of the fiducial through the equation (Ferreira, Tiago and Rasband, 2012):

$$Center\ of\ Mass\ (X/Y) = \frac{\sum(the\ inverse\ grey\ values\ of\ the\ pixel * the\ pixel\ (X\ or\ Y)\ coordinate)}{\sum(\ the\ inverse\ grey\ values\ of\ the\ pixel)} \quad (1).$$

Where, the positive translation of center of mass along the X-direction corresponds to the posterior direction; and the positive translation of center of mass of the Y-direction corresponds to superior directions.

Thus, the translation of the fiducial marks over time represented the amount of deformation or shrinkage for each mask in pixel units.

The total amount of deformation in the masks was measured by subtracting the fiducial coordinates of the first image obtained when the mask was mounted on the head phantom during cool down (0 hour) from the last fiducial coordinates of the last image (192 hour).

A potential source of error is associated with the variation in fiducial pixel coordinates, when the mask was replaced and imaged at each replacement. This error was assessed by imaging the mask after each of three re-positionings. At each re-positioning, the pixel coordinates of the fiducial point was determined using the center of mass algorithm. The sample standard deviation of the three sets of coordinates were used to estimate the reproducibility error of determining the location of the fiducial point on the mask.

Another measurement was performed that involved measuring the mask's height mounted on and off the head phantom. This was performed approximately 3 weeks after all the masks were formed. Each mask was remounted on the head phantom as described previously and the height from the base-frame to upper edge at all three locations (forehead, nose and chin) was measured using a precision vertical caliper tool. Next, the mask was remounted without the head phantom and the height was measured in the same manner. The percent deformation was obtained as following:

$$Percent\ deformation = \frac{height\ of\ the\ mask\ on\ the\ head\ phantom - \ height\ of\ the\ mask\ off\ the\ head\ phantom}{height\ of\ the\ mask\ on\ the\ head\ phantom} x100 \quad (2).$$

2.1.3. Scale factor determination

2.1.3.1. Experimental method of determining the scale factor

The translation of the fiducial points in the previous section determined the amount of mask deformation in pixel units. A scale factor is needed to convert from pixel units to millimeters. A graph scale was attached to a plate and mounted in place of the mask along the mask's sagittal plane on the optical bench at the same focal distance as the fiducials on the masks. The graph scale was then imaged by the camera as shown in Figure 10.

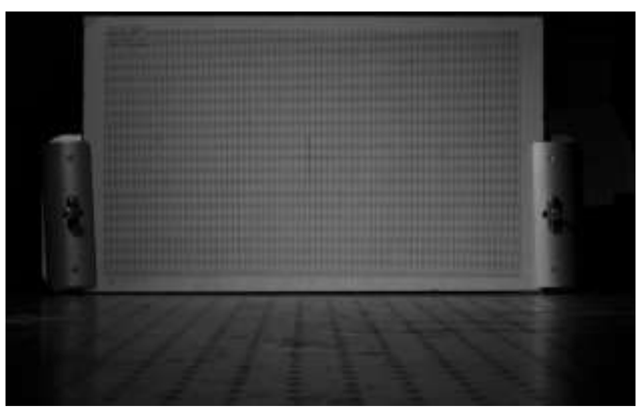

Figure 10. The graph scale imaged at the location of the fiducial points.

Using ImageJ to process the image, the number of pixels per mm was determined by sampling pixels along a straight line across the graph scale at various locations using the "straight line" tool. Gray value was plotted versus distance in pixels along each line (Figure 11).

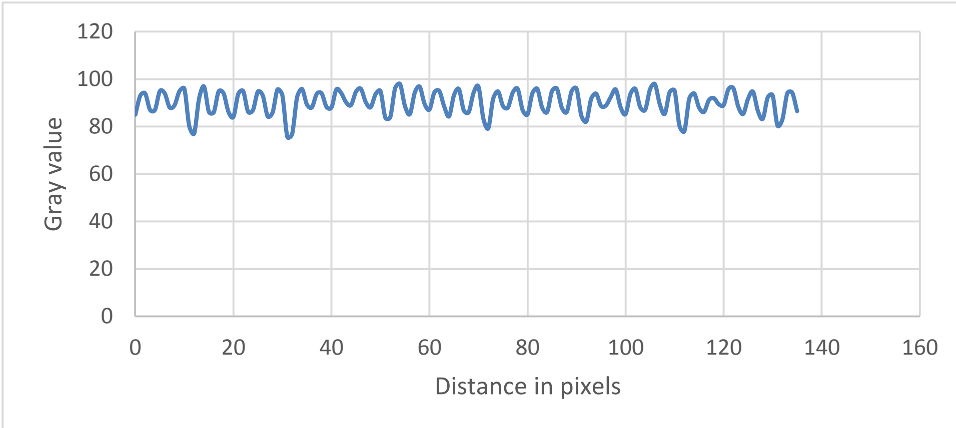

Figure 11. Relationship between the grey value and distance in pixels.

We can deduce from Figure 11 that the relationship between the gray value and the distance in pixels is a periodic function whose fundamental wavelength may be determined using Fourier analysis. The wavelength corresponds to the number of pixels per mm gradation on the scale.

One algorithm that computes the Fourier transform is the Fast Fourier transform. The transformation of the space-domain function to the frequency-domain function of graph data was performed using an online Fast Fourier transform(“Fast Fourier Transform Calculator,” n.d.). Sampled data points were first filtered using a Hamming windowing and the algorithm computed the power spectrum. The straight line sample of the graph paper was over 64mm (64 peaks) which consisted of 256 pixels. Since the power spectrum gives the amplitude of the individual frequency components of the sample, the power spectrum of the transform of Figure 11 has two peaks, symmetric about the Nyquist frequency.

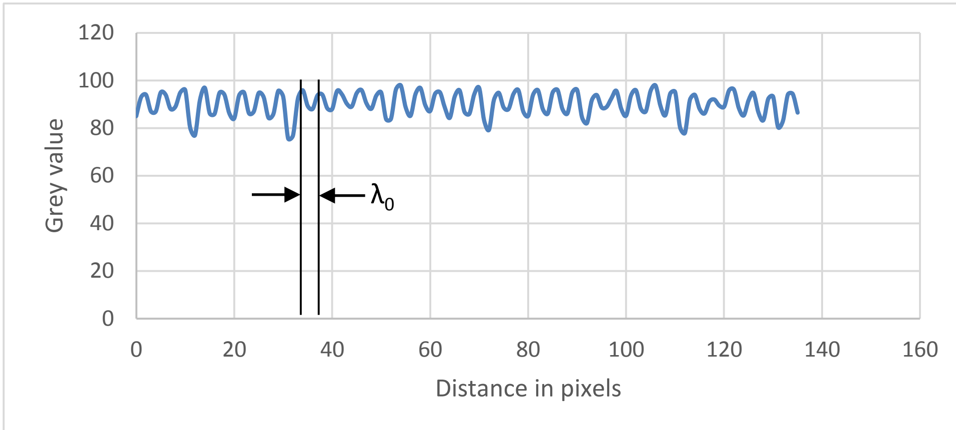

Figure 12. Real space.

Where, λ_0 = X pixels/oscillation.

The Nyquist frequency is obtained by dividing the number of samples by 2 ((256)/2 = 128).

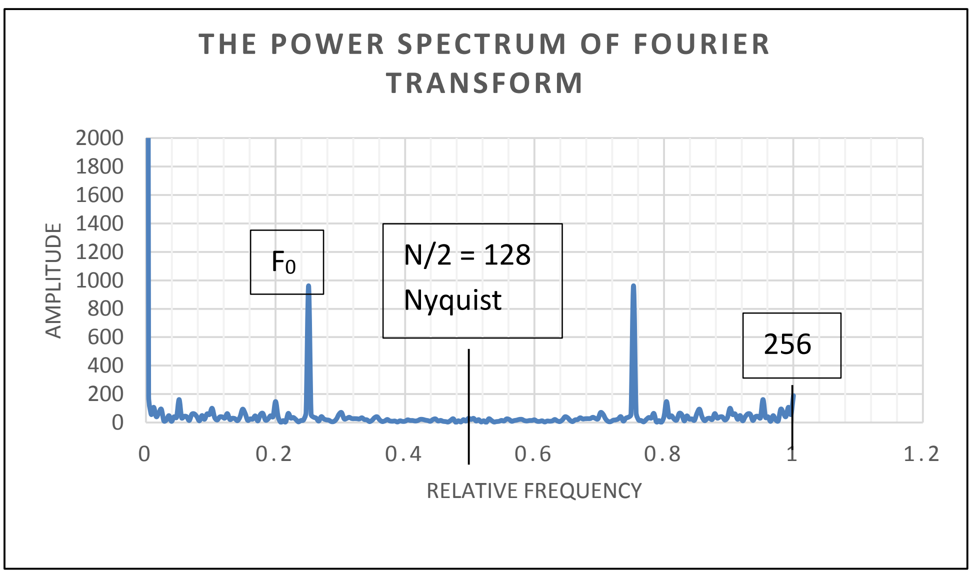

Figure 13. The power spectrum of the plot of the distance in pixels versus grey value on the graph scale.

Where F_0 = 1/X oscillation/pixels. F_0 is the number of pixels between two successive peaks (lines on the graph scale) which is the scale factor of converting from pixels to mms. 1 oscillation (two successive peaks) = 1 mm.

Therefore the amount of deformation in mm is

$$Amount\ of\ deformation\ in\ mm = \frac{pixel\ position\ of\ the\ fiducial\ at\ t_i - pixel\ position\ of\ the\ fiducal\ at\ t_0}{scale\ factor\ from\ Fourier\ transform} \qquad (3)$$

A potential source of error in scale determination is the alignment of the graph scale with the location of the fiducial points which were marked on the masks. Additionally, the focal distance to the fiducial points of different masks may have differed by a small amount. Therefore, the error in scale factor determination due to graph scale position was assessed by shifting the position of the graph scale from the original position of the fiducial points by 2.5cm backward or forward. At the shifted position, the graph scale factor was computed as outlined above. The difference between the two scale factors was calculated using the following equation:

$$difference\ =\ shifted\ \ value - original\ value \qquad (4)$$

Where the original value is the scale factor deduced from the graph scale placed at the original position.

2.1.3.2. Validation of the Fourier transform method for determining the scale factor

The technique of determining the scale factor using the Fourier transform method was evaluated by drawing a fiducial point on a card mounted on a three-axis micrometer in place of the graph scale (Figure 14). The Z axis of the micrometer was fixed, and the X and Y axes were translated separately by a sequence of sub-millimetre shifts up to 2 mm. Three photographs were acquired at each shift, so that the ratio of pixels per mm was determined from the slope of a plot of the fiducial point pixel location versus micrometer reading. The uncertainty of the slope was determined using the following equations:

$$S_{y/x} = \sqrt{\frac{\sum(y_i - \hat{y_i})^2}{N-2}}, \qquad (5)$$

Where $S_{y/x}$ is the uncertainty of the regression, $\hat{y_i} = mx + y\ intercept$, and N is the degree of freedom.

$$S_b = \frac{S_{y/x}}{\sqrt{\sum(x_i - \bar{x})^2}}, \qquad (6)$$

Where, x represented the reading from the micrometer, y is the center of mass of the fiducial point on the micrometer and S_b is the uncertainty of the slope, and $\bar{x}$ is the mean of measurements.

The fiducial point pixel location was determined using the center of mass algorithm implemented within ImageJ.

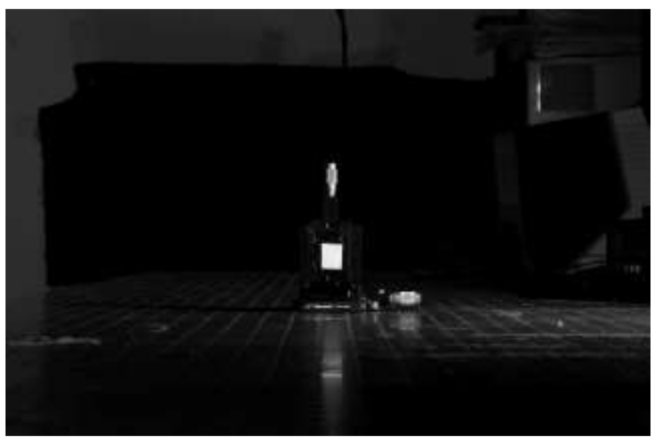

Figure 14. The three-axis micrometer attached with a card and mounted on the same location of the graph scale.

2.1.4. Error combination

Two sources of errors have been identified in the above experiment: one arose from error in re-positioning the graph scale away from the location of the fiducial points on the masks; the other emerged from the variation in determining the center of mass of the fiducial point marked on the mask after repeated repositioning the mask. Thus, the error in the amount of deformation in mm was determined by the following equation:

From the amount of deformation in mm equation deduced from section 2.1.2.4.,

$$Amount\ of\ deformation\ in\ mm = \frac{translation}{scale\ factor\ from\ Fourier\ transform}, \qquad (7)$$

the error is

$$\frac{\Delta\ amount\ of\ deformation\ in\ mm}{amount\ of\ deformation\ in\ mm} = \sqrt{\left(\frac{\Delta\ translation}{translation}\right)^2 + \left(\frac{\Delta\ repositioning\ the\ graph\ scale}{scale\ factor\ from\ Fourier\ transform}\right)^2}, \qquad (8)$$

Where, $translation = pixel\ posistion\ at\ t_i - \ pixel\ position\ at\ t_0$, and

$$\Delta\ translation = \sqrt{(\Delta\ pixel\ posistion\ at\ t_i)^2 - (\Delta\ pixel\ position\ at\ t_0)^2}. \qquad (9)$$

Where, Δ pixel position at t_i represents the error from the variation in determining the center of mass of the fiducial point marked on the mask after repeated repositioning the mask, and pixel position of the fiducial at t_i represents the fiducial coordinates of the image acquired at time t_i.

2.2. Pressure due to mask shrinkage

The pressure exerted by each mask on the head phantom at different locations after one week of shrinkage was investigated using pressure sensitive film.

2.2.1. An introduction to pressure sensitive film

2.2.1.1. Composition

Fuji manufactures pressure sensitive film, Prescale, for various ranges of pressure. For this work, extreme-low film type was used which covers the lowest range from 0.05 to 0.2 MPa, where 1MPa ≈ 10.2 kg g/ cm^2 and 1kg g = 9.8 m/s^2. The film consists of two different sheets: a layer of micro-encapsulated color forming substance called the transfer sheet covers one, while a layer of color developing substance called the developer sheet covers the other (Figure 15)(Fujifilm).

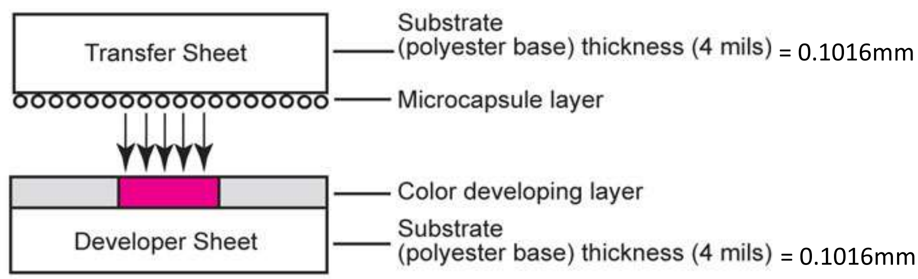

Figure 15.Description of the pressure measurement film(Fujifilm)**.**

According to range of the applied pressure, there are eight different types of pressure measurement film as it is illustrated in Table 4

Pressure Film Type	Pressure Range
Extreme Low	7.2 - 28 PSI (0.05 – 0.2 MPa)
Ultra Low	28 - 85 PSI (0.2 – 0.6 MPa)
Super Low	70 - 350 PSI (0.5 – 2.5 MPa)
Low	350 - 1,400 PSI (2.5 - 10 MPa)
Medium	1,400 - 7,100 PSI (10 - 50 MPa)
High	7,100 - 18,500 PSI (50 – 130 MPa)
Super High	18,500 - 43,200 PSI (130 - 300 MPa)

Table 4. Pressure ranges for different types of films(Fujifilm)**.**

2.2.1.2. How the film works

The film is used with the transfer sheet facing the developer sheet. When pressure is applied to the sheets, breakage of the microcapsules introduce a red color. The density of the red pixels is proportional to the pressure applied (Fujifilm).

2.2.1.3. How the film is calibrated

The pressure sensitive film can be calibrated using the Topaq® system. This system consists of a calibrated scanner and Windows software. The main function of the Topaq® system is to quantify the pressure applied to the pressure sensitive film. The Topaq® system images the film using the scanner and analyses the pressure presented on the image through the red color density. The Topaq® system provides a high resolution, color calibrated image and a lot of statistical information related to the tested film. Topaq® accuracy is within ±4% when it is used in tactile pressure measurements. The following table will illustrate the Topaq® system specifications (Sensor Products Inc).

Topaq® system specifications.	
Optical resolution	100-1000 DPI
Imaging area	12”-17” (A3)
Scanning mode	36-bit color
Weight	26 lbs (12 kg)
Power consumption	49 watts
Interface	USB
Scanning time	40 second
AC line voltage	100-240 VAC
Linearity	0-2 O.D.
Light source	Cold cathode lamp
Wavelength	400-750 nm
Absorbance range	0-3.2 O.D.
Image processing	Gamma adjustment, Filtering
Networkable	Unlimited number of users

Table 5. Topaq® system specifications (Sensor Products Inc)**.**

However, in this experiment, the Topaq system was not used. Instead, a special tool was made for the calibration of the applied pressure as illustrated in Figure 16. The rod moves vertically. The tool was mounted on the optical bench, with the film sandwiched between a circular neoprene disk placed on a flat level surface and the rod (figure 17). The neoprene disk was used in order to uniformly distribute the pressure on the film. Masses were placed on top of the rod. These masses were selected to match the pressure range of the film (0.05 MPa to 0.2 MPa). Each mass was allowed to apply a pressure for about 2 minutes at room temperature 24^{0}C and relative humidity of 39%. Pressure exerted by each mass was determined by the following equation:

$$P = \frac{M\ (Kg)\ X\ (980\,\frac{cm}{s^2})}{area\ (cm^2)} \qquad (10)$$

With an error $\frac{\Delta P}{P} = \sqrt{(\frac{\Delta M}{M})^2 + (\frac{\Delta area}{area})^2} \qquad (11)$

Where, $area$ is the area of the piece of neoprene disk which radius was 0.6350±5X10^{-4} cm.

Figure 16. Pressure sensitive film calibration tool.

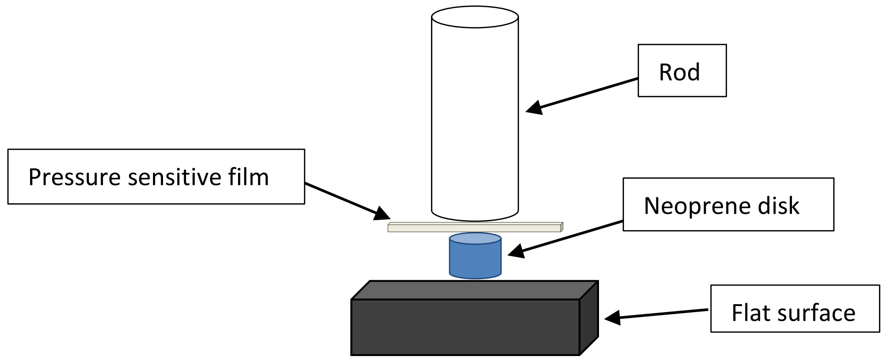

Figure 17. The description of using the piece of neoprene disk.

2.2.1.5. Features

Feature	Two-sheet type
Accuracy	±10% or less (measured by densitometer at $23^0C/73.4^oF$, 65%RH
Recommended temperature range	$15^0C – 30^0C$
Recommended humidity range	20%RH – 75%RH

Table 6. Features of the pressure sensitive film (Fujifilm)**.**

2.2.1.2. Film applications

Pressure sensitive film has been used in various fields, providing successful results as listed below(Fuji Prescale Film, 2001):

- Measuring a pressure distribution between two contact surfaces, gasket loading, regular force loading between any mechanical parts (Fuji Prescale Film, 2001).
- Measuring a pressure distribution under any heavy equipment, which is useful for heavy machinery hydraulic supports (Fuji Prescale Film, 2001).

- Determining a pressure pattern for parts that are facing contact in automotive field (Fuji Prescale Film, 2001).
- Measuring in the medical field, orthopedic diagnosis and biomechanics. For example, measurement of hand or finger pressure; making a correction on a foot pressure as if the foot was immobile and measurement of impact force (Fuji Prescale Film, 2001).

2.2.2. Data acquisition and analysis

After the calibration of the film was performed, pieces of the pressure sensitive film were cut and then taped carefully on the head phantom at three anatomical locations forehead, nose, and chin. Each mask was then mounted over the phantom and the film, and allowed to apply a pressure for about 2 minutes at a room temperature of 24^{0}C and 39% relative humidity. Afterward, the exposed films (calibration and measurement films) were scanned using an EPSON scanner. The scanner parameters are set out in Table 7.

Name of Input parameters	Input parameters
Film type	Reflective
Resolution	72 dpi
Configuration	No color correction
Image format	TIFF

Table 7. The scanner parameters.

All the scanned images were separated into three color channels red, green, and blue. The red channel was inverted as shown in Figure 18.

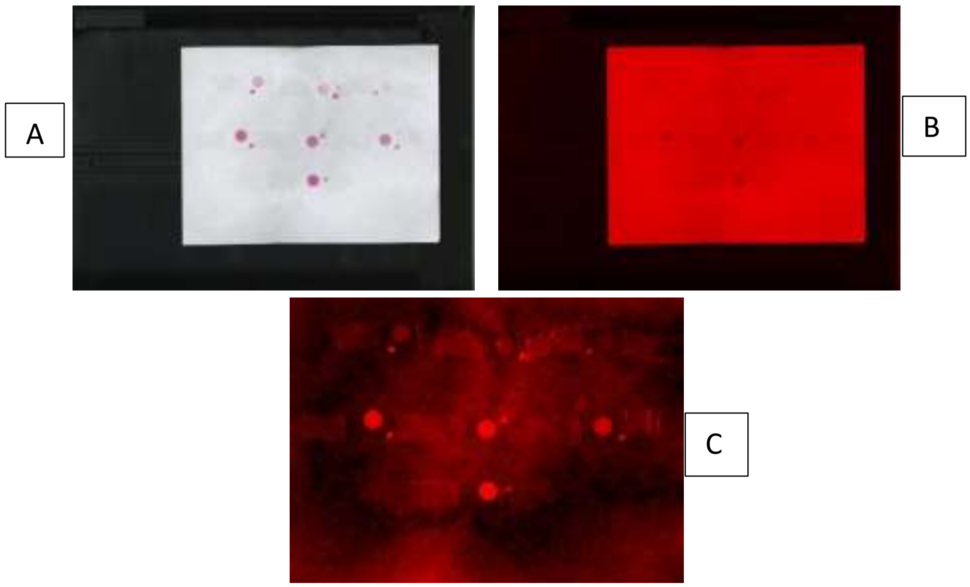

Figure 18. A sample of the scanned pressure sensitive film displayed using the red (B) and inverted red color channels (C) of the original film (A).

The red color channel was selected since the pressure sensitive film develops a red color (Figure 18). In ImageJ software, darker pixels have smaller gray or red values. Therefore, all images of the film were inverted so that the pixels that originally appear as white are assigned a low value while these that appear red are assigned a high red value.

The inverted red image of the calibration film was analysed as follows: circular area was selected using ImageJ software as shown in Figure 19. The median inverted red value was taken to represent the pressure corresponding to each circle. The circles shown in the image correspond to pressures of 0.03, 0.04, 0.05, 0.06, 0.08, 0.1, 0.12, 0.15, and 0.17 MPa. The inverted red value was plotted as function of the pressure to determine an equation to convert from inverted red value to pressure in units of MPa.

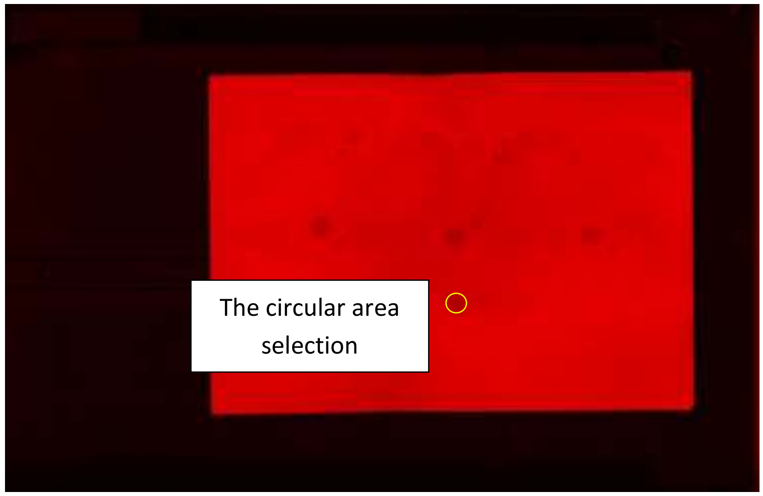

Figure 19. The circular area selected using ImageJ software.

The measurement films were analysed as follows: all the images of the films were separated into three image channels. The red channel was inverted as before (Figure 20).

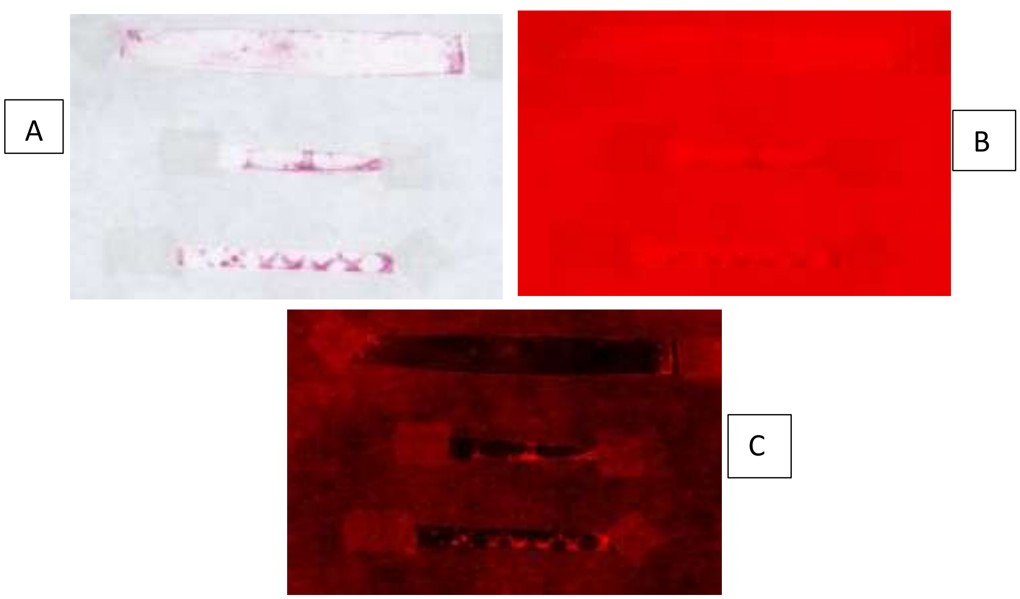

Figure 20. Pressure sensitive film (A), results displayed using red (B) and inverted red color channel (C). The film strips ordered from top to bottom correspond to measurements taken at the forehead, nose and chin respectively.

In Figure 20, we observe that the pressure varies across each film. Therefore, the films were analysed by selecting areas that appear to have the highest density of red, and finding the median inverted pixel value of that area. Thus, for our example (the chin film in Figure 20), many areas were sampled each giving an inverted median pixel value representing a different pressure. These were averaged and a sample standard deviation of the medians was computed. The averaged median and the standard deviation of the films were converted to pressure units (MPa) using the equation deduced from the plot of median inverted red value versus pressure.

2.2.2.1. Statistical analysis of the pressure averages

One-way analysis of variance (ANOVA) or F test was performed to compare between the averaged medians of forehead films, nose films and chin films separately. F test is used to compare among three or more averages or means by accepting or rejecting a null hypothesis. The null hypothesis asserts that the means are equal (Bluman, 2009). The assumptions for the F test are listed in Table 8.

The assumption for the F test for comparing three or more means
1- The population from which the samples were obtained must be normally or approximately normally distributed.
2- The samples must be independent of one another.
3- The variances of the populations must be equal.

Table 8. The assumption for the F test for comparing three or more means (Bluman, 2009)**.**

If a continuous variable is obtained from a single measurement, then the histogram of the variable will have a normal distribution (Campbell, 2006) with a standard deviation from the mean . Thus, in this experiment, if N measurements of pressure were obtained from the measurement films, then the histogram of those N measurements of pressure will have a normal distribution with a standard deviation from the mean of the pressure. The second assumption of the F test is satisfied since the measured pressure due to one mask is independent of that due to another. The last assumption is satisfied since the technique of measuring the pressure was identical for all masks giving equal variances of the populations.

F test estimates two different variances of the populations, one is called between-group variance and the other is called within-group variance. The between-group variance finds the variance of the means of groups, while the within-group variance finds the variance of all data. If the F value is greater than the critical value, which is inferred based on two kinds of degree of freedom measures [between-group variance (d.f.N. = *k* - 1) and within-group variance (d.f.D. = N - *k*)], where *k* and N are the number of groups and number of samples respectively, from the table of F distribution at 95% confidence interval (α = 0.05), then the means of the population are significantly different (rejecting the null hypothesis) and vice versa (Bluman, 2009).

Computing F value:

$$F = \frac{MS_B}{MS_W} \qquad (12)$$

Where, MS_B and MS_W are the mean square of the between-group variance and the mean square of the within-group variance respectively.

$$MS_B = \frac{SS_B}{k-1} \qquad (13)$$

Where, SS_B is the sum of the squares between groups and *k* is the number of groups.

$$MS_W = \frac{SS_W}{N-k} \qquad (14)$$

Where, SS_W is the sum squares within the groups and N is the sum of the sample size for groups (Bluman, 2009).

Using Excel software, the F test was applied to all forehead films, nose films, and chin films.

If the null hypothesis is rejected by the F test, then there is a mean or means that differ significantly. A test called the Scheffe test was applied between all possible pairs of masks to distinguish such a mean or means (Bluman, 2009).

The formula for the Scheffe test is

$$F_s = \frac{(\overline{X_i} - \overline{X_J})^2}{s_W^2[(\frac{1}{n_i})+(\frac{1}{n_j})]} \qquad (15)$$

Where, $\overline{X_i}$ is the mean of a sample compared with the mean of another $\overline{X_J}$, n_i, n_j are the sample sizes of the respective means and S^2_w is the within-group variance equal to $\frac{\sum(n_i-1)\, s_i^2}{\sum(n_i-1)}$, where s_i^2 is the variance of a group of population. The critical value of Scheffe test is F' = the critical value for the F test multiplied by *k-1*, where *k* stands for the number of groups (Bluman, 2009).

If the F_s value is greater than the critical value F' then the compared means are not equal (Bluman, 2009).

3. CHAPTER 3: Results and discussion

3.1. Pixel position determination

The error associated within the center of mass pixel coordinates of a fiducial point marked on a mask was determined by remounting and replacing the mask three times. After each replacement the pixel coordinates are determined and averaged. The error in this value is represented by the standard deviation of 0.022 pixels.

3.2. Scale factor determination

An online Fast Fourier transform application was used to determine the fundamental frequency (F_0) of the power spectrum.

The relative frequency of the fundamental peak in the power spectrum was found to be F_0 = 0.250±0.004 Pixel^{-1}.

The error in F_0 is determined by the resolution of frequency which corresponds to 1/N where N = 256 is the number of samples.

The scale Factor = 1/f = 4.00±0.004 pixels/mm, where the relative error in f of 1.6% is preserved.

When the graph scale was shifted by 2.5cm from the original location of the fiducial points marked on the masks, the difference on the scale factor was

$$difference\ =\ shifted\ \ value - original\ value$$

$$= 4.06\ \frac{pixels}{mm}\ -\ 4\ \frac{pixels}{mm}\ = 0.06 \text{ pixels/mm}$$

This corresponds to the error in scale factor determined from the power spectrum.

Since the scale factor of the shifted value was equal to 4.06 pixels/mm then the corresponding frequency = 0.246 pixel^{-1}. The scale factor of the original value was 4 pixels/mm with a corresponding frequency of is 0.25pixel^{-1}. Then by subtraction we will have

F_1- F_0 = 0.25-0.246=0.004 pixel^{-1} which corresponds to the resolution of the Fourier analysis.

In other words, for our sample length of 256 pixels, Fourier analysis can only resolve two separate peaks separated by of 0.004 pixel^{-1}; shifting the graph scale by

2.5cm from the original position shifted the peak to the next neighboring channel in power spectrum. furthermore, when the graph scale was moved by less than 2.5cm, the Fourier transform did not distinguish between the frequency of the resulting peak and the original peak.

3.3. Validating Fourier transform scale factor using a micrometer

The plot of the fiducial point pixel location versus micrometer reading is shown in Figure 21.

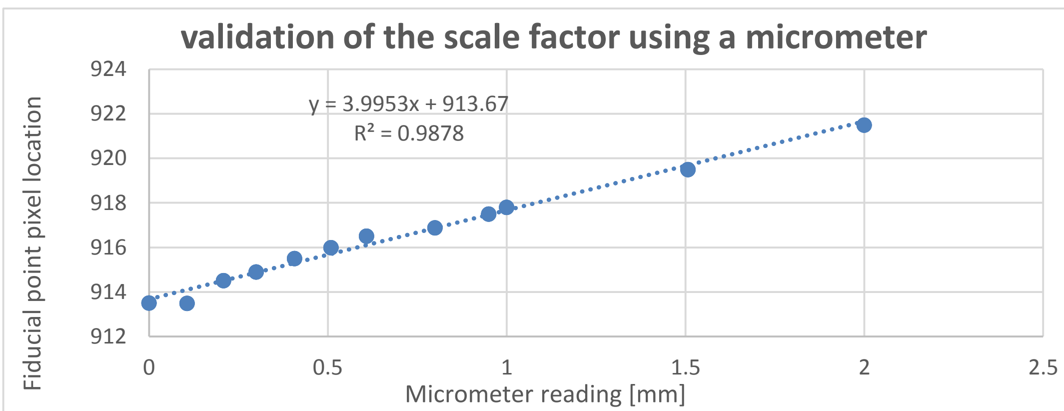

Figure 21.The plot of the fiducial point pixel location versus micrometer reading.

We can infer from Figure 17 that the slope of the line is 3.995 which is the ratio of pixels per mm. The uncertainty of the regression line of Figure 17 was

$$S_{y/x} = \sqrt{\frac{\sum(y_i - \hat{y_i})^2}{N-2}} = 0.2602,$$

Where, $\hat{y_i} = 3.9953x + 913.67$, and N = 36

Therefore, the uncertainty of the slope or the scale factor was

$$S_b = \frac{S_{y/x}}{\sqrt{\sum(x_i - \bar{x})^2}} = 0.0763,$$

Thus, the scale factor deduced from the movement of the micrometer was 3.995±0.076 pixels/mm.

The Fourier transform scale factor (4.00±0.06pixel/mm) and the micrometer scale factor (4.00±0.08 pixels/mm), agree to within measurement error.

3.4. Error combination

As mentioned in section 2.1.4. the two sources of errors were: the error due to scale factor uncertainty (4.00±0.06 pixels/mm), and the error due to determining the deformation in pixel coordinates in (0.022 pixel). Combining these two errors, gives the error in the amount of deformation in mm.

Hence, from equations 8 and 9, the error in the amount of deformation in mm is

$$\frac{\Delta\, amount\ of\ deformation\ in\ mm}{amount\ of\ deformation\ in\ mm} = \sqrt{\left(\frac{0.031\ pixels}{translation}\right)^2 + \left(\frac{1.6\%}{4\ pixels/mm}\right)^2},$$

3.5. Mask deformation in posterior direction

The following figures, Figure 22, Figure 23 and Figure 24, show a comparison of the amount of deformation of the entire masks at forehead, nose, and chin with the calculated error referenced to time = 0 which corresponds to the mask formed on the head phantom.

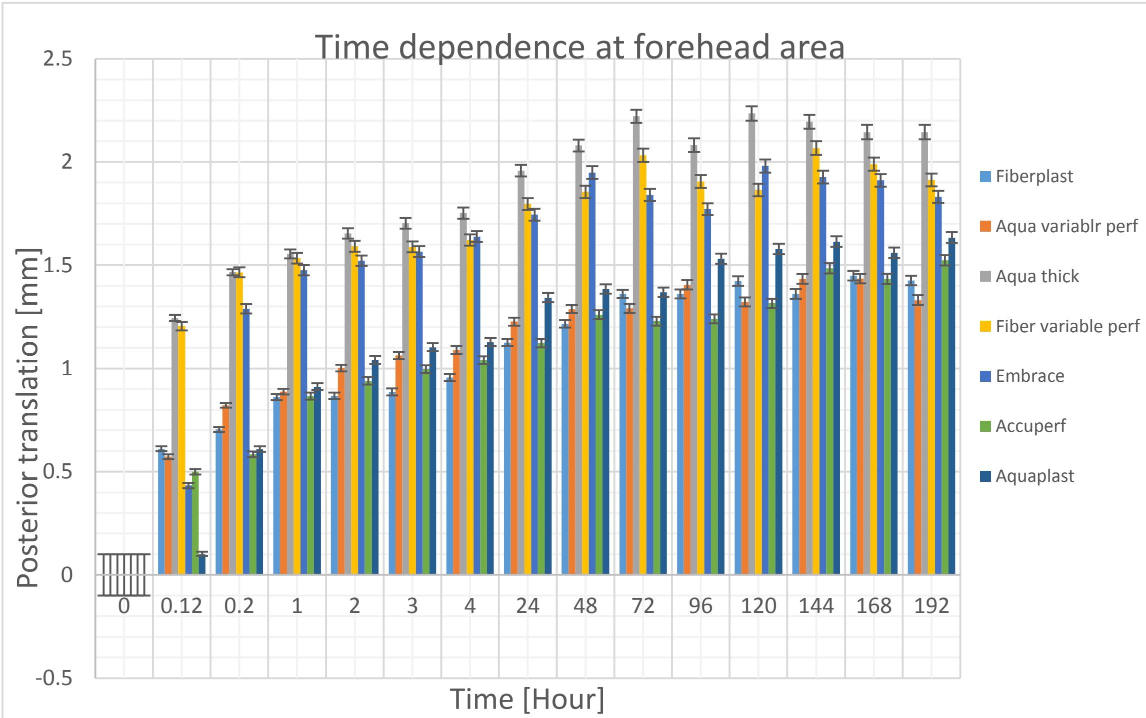

Figure 22. The amount of deformation in posterior direction for all masks at forehead area.

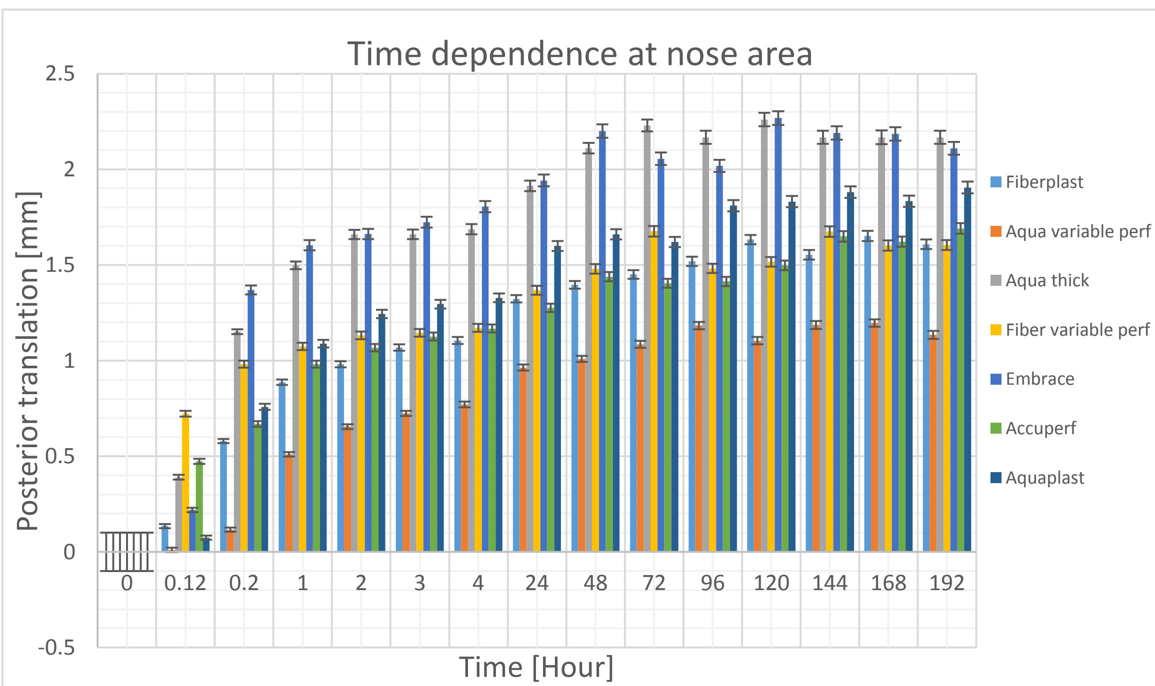

Figure 23. The amount of deformation in posterior direction for all masks at nose area.

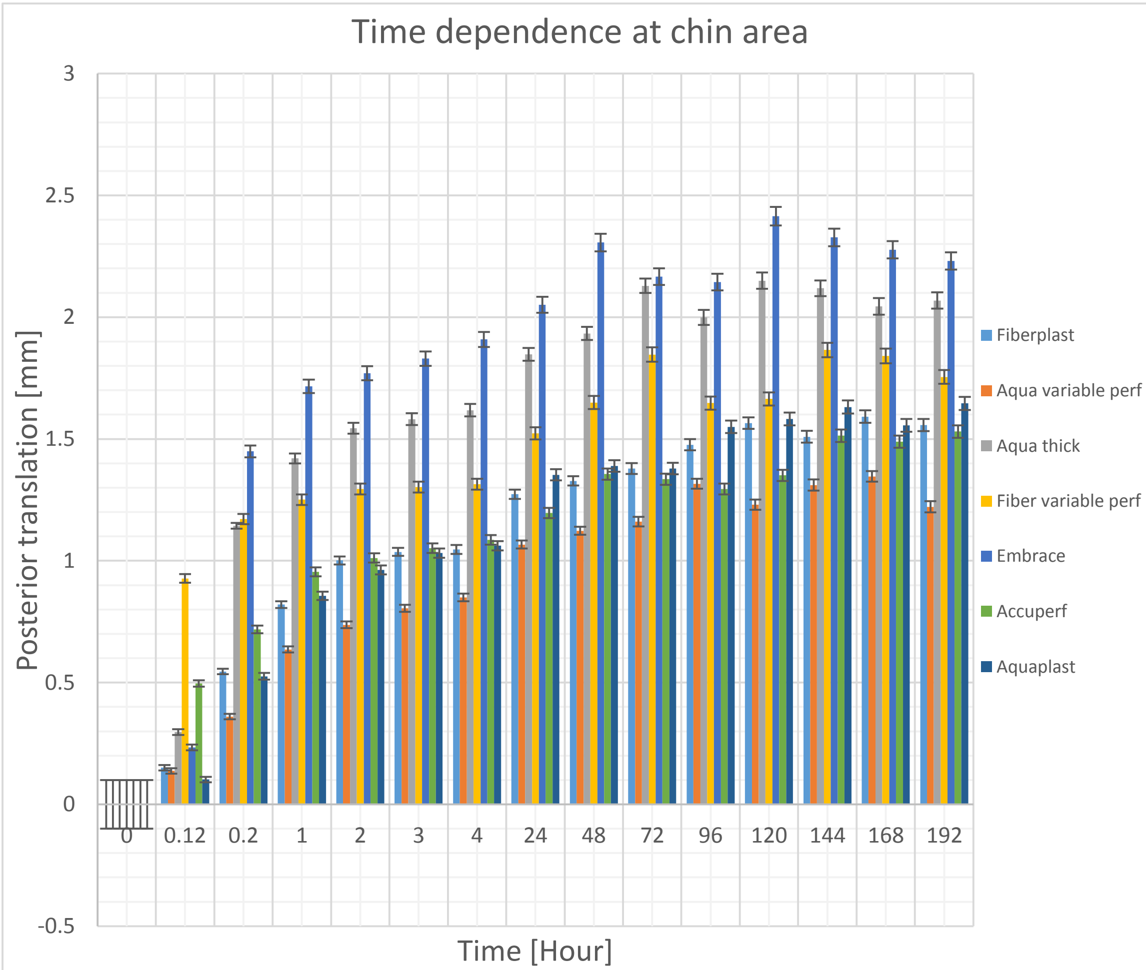

Figure 24. The amount of deformation in posterior direction for all masks at chin area.

The 0 hour entry in the three Figures above refers to the first image taken when the mask was still warm on the head phantom. This was used as a reference time for the following images by subtracting the fiducial coordinates of the following images from the fiducial coordinates of the reference image. The error at 0 hour is due to the re-positioning the mask on the plastic mounting tray after the removal of the head phantom, which was estimated to be 0.1mm.

Figures 22, 23 and 24 indicate that the deformation/shrinkage in all masks began at the formation of the masks on the head phantom, and that the amount of deformation was not equal among all of the masks. After 0.12 hours, the amount of deformation increased until about 48 hours, and then remained constant.

The following table sets out the total posterior translation from the time when the mask was taken out of the water bath to hour 192 with its calculated error. All masks are sorted from most to least shrinkage amount at nose area.

The total amount of deformation in posterior direction from 0-192 hour [mm]			
Mask Model	**Forehead**	**Nose**	**Chin**
Aqua thick	2.144±0.022 (0.982%±0.0001%)	2.167±0.024 (0.849%±0.0001%)	2.068±0.024 (0.878%±0.0001%)
Embrace	1.831±0.023 (0.839%±0.0001%)	2.109±0.02 (0.838%±0.0001%)	2.231±0.021 (0.957%±0.0001%)
Aquaplast	1.632±0.03 (0.746%±0.0001%)	1.905±0.025 (0.758%±0.0001%)	1.646±0.03 (0.705%±0.0001%)
AccuPerf	1.523±0.03 (0.697%±0.0001%)	1.691±0.032 (0.674%±0.0001%)	1.530±0.03 (0.65%±0.0001%)
Fiberplast	1.0426±0.024 (0.653%±0.0001%)	1.608±0.026 (0.639%±0.0001%)	1.557±0.024 (0.666%±0.0001%)
Fiber variable perf	1.913±0.034 (0.874%±0.0001%)	1.604±0.033 (0.630%±0.0001%)	1.754±0.032 (0.752%±0.0001%)
Aqua variable perf	1.330±0.025 (0.609%±0.0001%)	1.135±0.03 (0.446%±0.0001%)	1.221±0.025 (0.523%±0.0001%)

Table 9. The total amount of deformation in posterior direction for all masks. The percentage in the brackets are the percent deformation computed by Equation 2.

The following table sets out the amount of deformation from 0 hour to 0.12 hour which corresponded to the deformation when the mask was becoming harder on the head phantom.

The amount of deformation from 0 hour to 0.12 hour in posterior direction			
Mask Model	Forehead	Nose	Chin
Aqua thick	1.245±0.012 (0.569%)	0.389±0.01 (0.154%)	0.296±0.009 (0.127%)
Embrace	0.432±0.010 (0.197%)	0.218±0.008 (0.087%)	0.234±0.014 (0.100%)
Aquaplast	0.100±0.008 (0.0456%)	0.074±0.008 (0.029%)	0.102±0.008 (0.044%)
AccuPerf	0.499±0.010 (0.228%)	0.473±0.010 (0.188%)	0.496±0.010 (0.21%)
Fiberplast	0.610±0.008 (0.279%)	0.135±0.008 (0.054%)	0.150±0.008 (0.064%)
Fiber variable perf	1.205±0.019 (0.552%)	0.722±0.013 (0.282%)	0.927±0.015 (0.396%)
Aqua variable perf	0.572±0.008 (0.262%)	0.0102±0.008 (0.004%)	0.137±0.008 (0.059%)

Table 10. The amount of deformation from time 0 hour to 0.12 hour (cooling of the mask on the head phantom and re-mounting onto the same base-plate). The percentages in the brackets are the percent deformation calculated using Equation 2.

The following table sets out the amount of deformation from 0.12 hour to 192 hour which corresponded to when the mask was already cooled down and removed from the head phantom.

The amount of deformation from 0.12-192 hour in posterior direction [mm]			
Mask Model	Forehead [mm]	Nose [mm]	Chin [mm]
Aqua thick	1.000±0.036 (0.457%)	1.778±0.034 (0.708%)	1.772±0.033 (0.758%)
Embrace	1.400±0.03 (0.640%)	1.890±0.033 (0.752%)	1.997±0.039 (0.853%)
Aquaplast	1.532±0.026 (0.702%)	1.830±0.030 (0.719%)	1.544±0.027 (0.662%)
AccuPerf	1.024±0.026 (0.468%)	1.218±0.028 (0.478%)	1.034±0.026 (0.443%)
Fiberplast	0.814±0.023 (0.372%)	1.473±0.025 (0.577%)	1.406±0.025 (0.596%)
Fiber variable perf	0.71±0.035 (0.325%)	0.882±0.028 (0.351%)	0.827±0.031 (0.351%)
Aqua variable perf	0.8±0.024 (0.367%)	1.125±0.020 (0.447%)	1.084±0.022 (0.464%)

Table 11. The amount of deformation after initial cooling and remounting the mask. The percentage in the brackets are the percent deformation calculated using Equation 2.

Aquaplast and Embrace masks shrank the most. The former at the forehead region by amount of 1.532±0.026mm, and the latter at the nose and chin regions by values of 1.890±0.033mm and 1.997±0.039mm, respectively (Table 11). Fiber variable perf shrank the least, having shrank 0.71±0.035mm, 0.882±0.028mm, and 0.827±0.031mm, over the same regions respectively (Table 11).

The following table illustrate the percent deformation for all masks computed as outlined in section 2.1.2.4. Equation 2.

The percent deformation for all masks			
Mask Model	**Forehead**	**Nose**	**Chin**
Aqua thick	2.33%±0.008% (0.982%)	1.373%±0.007% (0.849%)	0.944%±0.008% (0.878%)
Embrace	1.639%±0.008% (0.839%)	0.887%±0.007% (0.838%)	0.861%±0.008% (0.957%)
Aquaplast	1.488%±0.008% (0.746%)	0.837%±0.007% (0.758%)	0.808%±0.008% (0.705%)
AccuPerf	1.326%±0.008% (0.697%)	0.810%±0.007% (0.674%)	0.788%±0.008% (0.65%)
Fiberplast	1.185%±0.008% (0.653%)	0.726%±0.007% (0.639%)	0.700%±0.008% (0.666%)
Fiber variable perf	1.720%±0.008% (0.874%)	0.696%±0.007% (0.630%)	0.678%±0.008% (0.752%)
Aqua variable perf	1.069%±0.008% (0.609%)	0.595%±0.007% (0.446%)	0.538%±0.008% (0.523%)

Table 12. The percent deformation for all masks. The percentage in the brackets are the percent deformation taken from Table 9.

By comparing between Table 12 and Table 9, both Tables showed that Aqua thick mask had the greatest deformation at nose. Whereas, the least deformation was due to Aqua variable perf according to Tables 12 and 9 at nose. In addition, the sequences of values ranked from the greatest to the least deformation are similar between Tables 12 and 9, although the percent of deformation is different.

Table 10 showed some masks are consistent across forehead, nose and chin which for example are Aquaplast and AccuPerf as it was expected. However Fiberplast showed inconsistency across forehead, nose and chin, indicating there was systematic error. Further, since Fiber variable perf and Aqua variable perf have similar perforation pattern, the amount of shrinkage are expected to be consistent, but were not based on Table 10, which indicates systematic errors.

Furthermore, Table 11 showed Fiber variable perf was the least deformed amongst all the masks, indicating that most of the deformation occurred during the time of cooling the mask on the head phantom which made Fiber variable perf the most deformed based on Table 10. However, Table 12 showed Fiber variable perf the second least deformed mask. Further, the greatest deformation at nose was due to Embrace based on Table 11, while Table 12 showed Embrace mask the second deformed mask. In addition, because the masks were not removed from the plastic mounting tray after they were replaced when the head phantom was removed, the amount of shrinkages for all masks on forehead, nose and chin according to Table 11 are consistent.

Table 12 shows that the percent deformation at the forehead for all masks is roughly double that at the nose and chin. This indicates that there was a systematic error in the caliper measurement of the deformation.

These result suggest that systematic errors may be presented in either of the two experiment (measuring shrinkage using time-lapse photography technique or using the caliper to measure the difference in height on and off the head phantom) that led to the big differences in the percent of deformation. These errors may be due to replacing the mask appropriately on the optical bench after the removal of the head phantom, or due to other errors that were not appreciated.

3.6. Masks deformation in superior/inferior directions

The following plots illustrate the amount of deformation for all masks in superior/inferior directions with the error calculated as described earlier. Negative values correspond to the inferior direction.

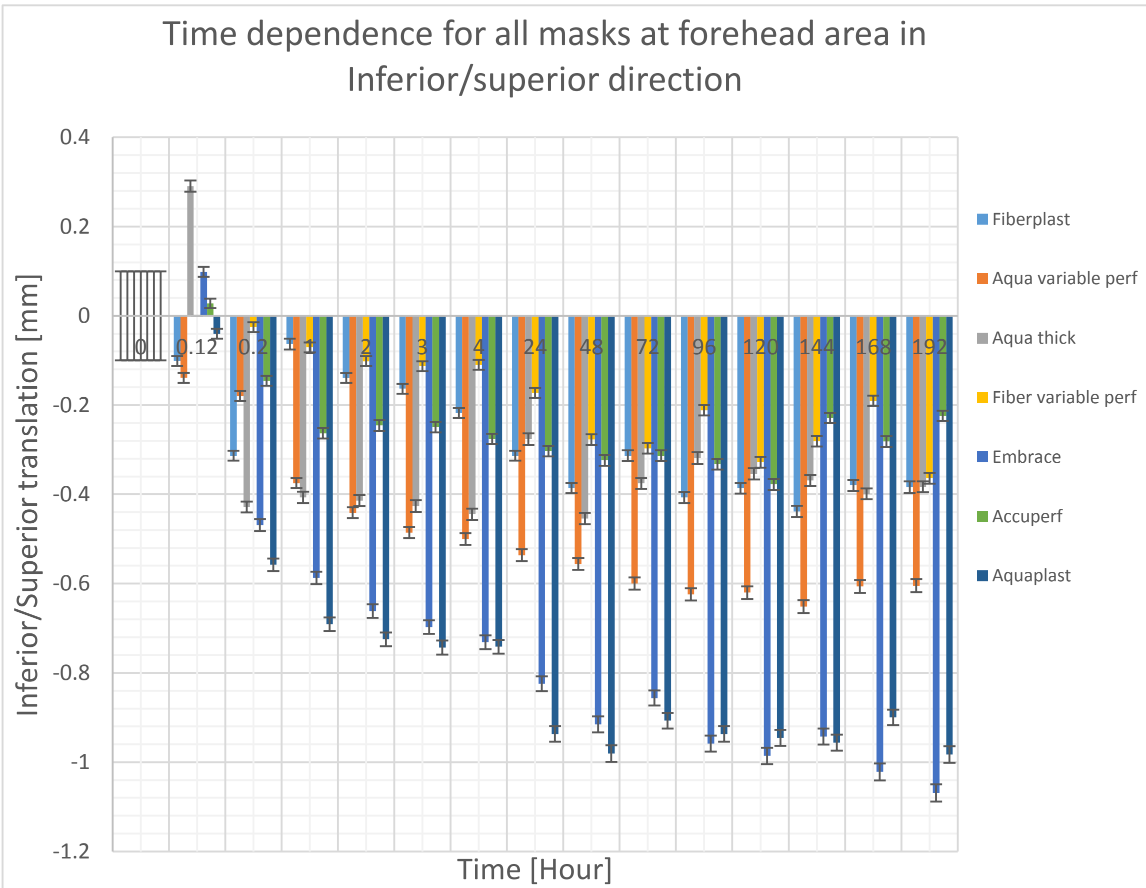

Figure 25. Masks deformation in superior/inferior directions at forehead area.

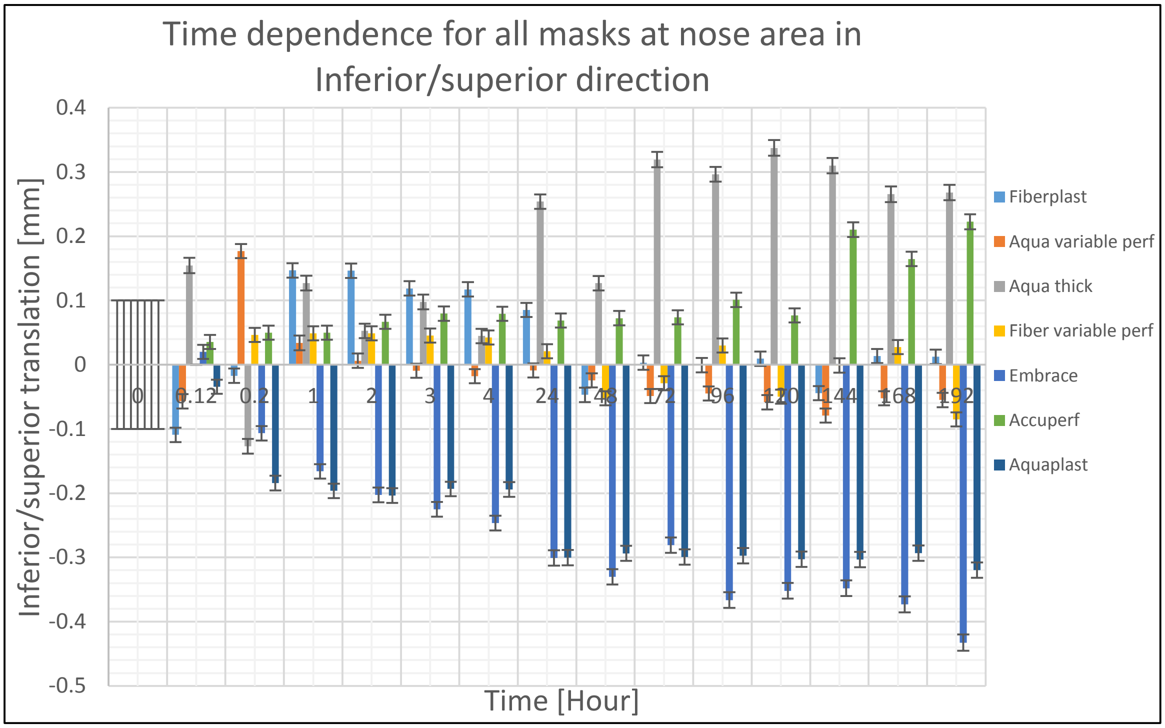

Figure 26. Masks deformation in superior/inferior directions at nose area.

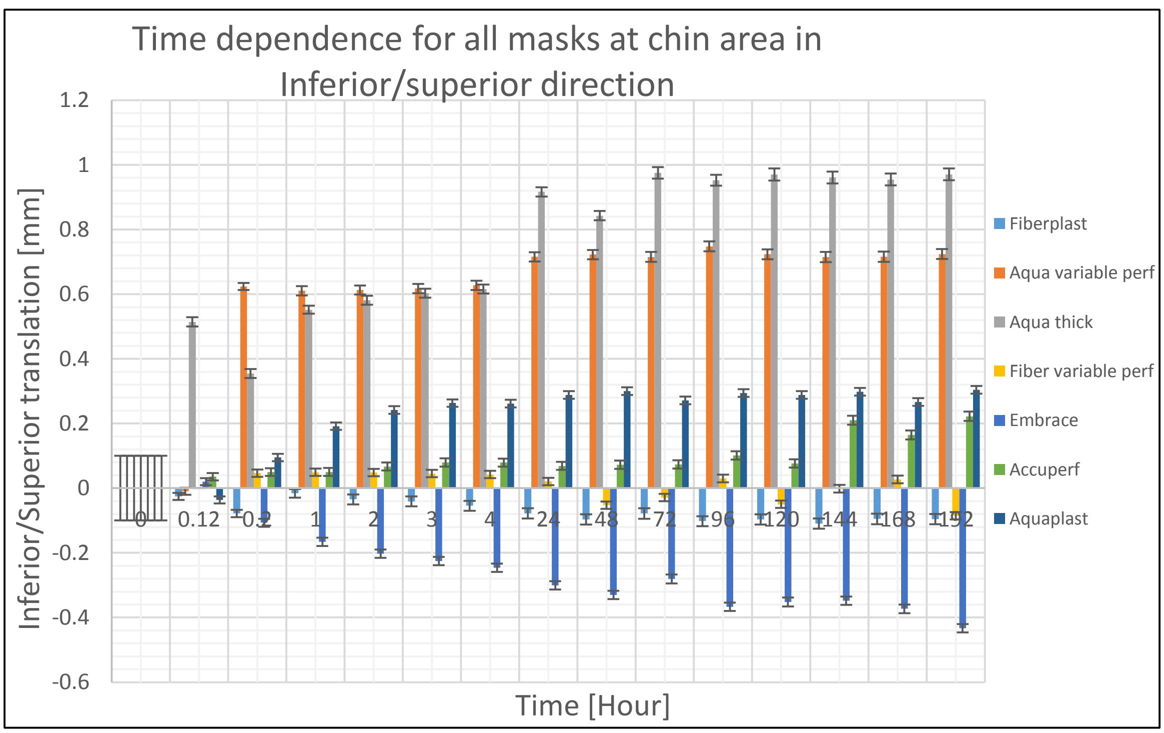

Figure 27. Masks deformation in superior/inferior directions at chin area.

All masks started to deform in superior/inferior directions, from the time the mask was formed on the head phantom until about 48 hours as shown in Figures 25, 26 and 27. The greatest amount of deformation was seen in Aqua thick and Embrace. Embrace was the most deformed at forehead and nose areas, while Aqua thick was the most deformed at chin area. The least amount of deformation was exhibited by Fiberplast, Fiber variable perf, and AccuPerf. AccuPerf mask, Fiberplast, and Fiber variable perf showed the least deformation at forehead, nose, and chin respectively. The negative values in Table 13 correspond to the deformations in the inferior direction. The total amount of deformation for all masks in superior/inferior direction are set out in Table 13.

The total amount of deformation in superior/ inferior direction for all masks [mm]			
Mask Model	**Forehead**	**Nose**	**Chin**
Fiberplast	-0.384±0.010	0.012±0.008	-0.096±0.010
Aqua variable perf	-0.604±0.012	-0.055±0.008	0.724±0.013
Aqua thick	-0.383±0.009	0.268±0.009	0.970±0.016
Fiber variable perf	-0.364±0.009	-0.085±0.008	-0.085±0.008
Embrace	-1.069±0.017	-0.432±0.010	-0.433±0.015
AccuPerf	-0.224±0.008	0.222±0.008	0.222±0.011
Aquaplast	-0.983±0.016	-0.320±0.009	0.304±0.009

Table 13. The total amount of deformation for all masks at all areas in superior/inferior direction.

3.7. Pressure due to shrinkage

3.7.1. Calibration of the pressure sensitive film

The following chart shows the relationship of the pressure as a function of the inverted red value.

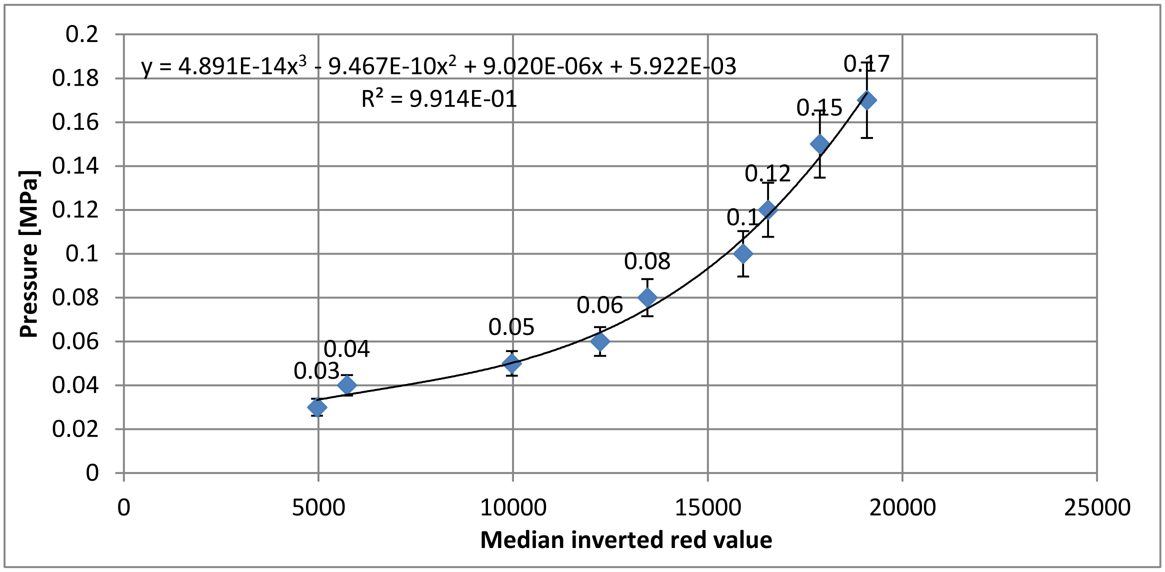

Figure 28. The calibration of the pressure sensitive film.

A third-order polynomial is used to fit the film response.

The equation in Figure 28

$$P = 4.891X10^{-14}(x^3) - 9.467X10^{-10}(x^2) + 9.020X10^{-6}(x) + 5.922X10^{-3} \quad (16)$$

was used to fit the pressure P in MPa to the median inverted red values x for the calibrations films.

3.7.2. Averaged median pressure at the forehead location for all masks

The following table illustrates the median and the averaged median pressures for all masks at the forehead location listed from the highest to lowest.

The median and averaged median pressure [MPa] for all masks at the forehead location							
Median	Fiber variable perf	Embrace	Aqua thick	Aquaplast	Fiberplast	AccuPerf	Aqua variable perf
1	0.135	0.048	0.049	0.045	0.044	0.041	0.035
2	0.091	0.055	0.050	0.043	0.044	0.041	-------
3	0.108	0.042	-------	-------	0.044	-------	-------
4	0.111	0.055	-------	-------	-------	-------	------
Average	0.112	0.0499	0.0498	0.0442	0.044	0.041	0.035
SD	0.0182	0.006	0.0004	0.0016	0.0001	0.0004	-----

Table 14. The median and the averaged median pressure for all masks at the forehead location with the sample standard deviation.

In order to find whether the averaged median pressure for mask at the forehead location is not significantly different, the F test was applied using Excel software. The following table illustrates the result of F test (ANOVA) at the forehead location.

Anova: Single Factor				
Mask name	*Count*	*Sum*	*Average*	*Variance*
Fiberplast	3	0.131	0.044	1.4E-08
Aqua variable perf	1	0.035	0.035	------------
Aqua thick	2	0.099	0.049	1.54E-07
Fiber variable perf	4	0.446	0.112	0.0003
Embrace	4	0.199	0.049	3.59E-05
AccuPerf	3	0.123	0.041	1.41E-07
Aquaplast	2	0.088	0.044	2.55E-06

Table 15. The averaged median pressure with the variance of the median for all masks at the forehead location.

ANOVA test result at the forehead location					
Source of Variation	*SS*	*df*	*MS*	*F*	*F critical*
Between Groups	0.014	6	0.002	25.731	2.996
Within Groups	0.001	12	9.24E-05	--------	--------
Total	0.015	18	--------	--------	--------

Table 16. The result of F test (ANOVA) at the forehead location.

Where, SS is the sum square, df is the degree of freedom, MS is the mean square, F is the F test value and F critical is α (the confidence interval at 95%) = 0.05.

Table 16 indicates that, the averaged median pressures for all or some of the masks at the forehead location were not equal since the F test value is greater than the F critical value. We therefore applied the Scheffe test (F_s value) in order to find the averaged median pressures that were different from the others. The following table illustrates the results of Scheffe test using equation 15.

The critical value (F') of the Scheffe test was computed to be 17.976 as outlined above.

Table of F_s values for comparison between masks						
Mask name	**Aqua variable perf**	**Aqua thick**	**Fiber variable perf**	**Embrace**	**AccuPerf**	**Aquaplast**
Fiberplast	0.649	0.467	85.393	0.696	0.125	0.002
Aqua variable perf	------------	1.611	51.050	1.967	0.308	0.634
Aqua thick	------------	---------	55.191	0.0002	1.001	0.335
Fiber variable perf	------------	---------	------------	82.439	92.537	65.565
Embrace	------------	---------	------------	------------	1.472	0.467
AccuPerf	------------	---------	------------	------------	-----------	0.134

Table 17. Table of F_s values for comparison between masks at the forehead location.

Tables 17 indicates that the F_s value for Fiber variable perf was significantly different from the others since its F_s value is greater than the critical value F'. The averaged median pressure of Fiber variable perf is the greatest among the masks. All other F_s values are smaller than the critical value which therefore indicates that the averaged median pressures were not significantly different.

3.7.3. Averaged median pressure for all masks at the nose location

The following table sets out the median and averaged median pressure value for all mask at the nose location listed from the highest to the lowest.

The median and the averaged median pressure [MPa] for all masks at the nose location							
Median	Aqua thick	Aqua variable perf	Fiber variable perf	Fiberplast	AccuPerf	Embrace	Aquaplast
1	0.178	0.182	0.173	0.139	0.085	0.092	0.058
2	0.144	0.148	0.143	0.058	0.084	0.066	0.078
3	0.084	0.081	0.136	-------	0.046	0.048	0.053
4	-------	0.116	0.086	-------	-------	-------	0.055
5	-------	-------	0.059	-------	-------	-------	-------
6	-------	-------	0.056	-------	-------	-------	-------
Average	0.135	0.132	0.109	0.098	0.072	0.069	0.061
SD	0.047	0.043	0.048	0.056	0.022	0.0219	0.0114

Table 18. The median and the averaged median pressure [MPa] for all masks at the nose location with the sample standard deviation.

The following tables will illustrate the F test (ANOVA) for the averaged medians pressures of the masks at the nose location using Excel software.

Anova: Single Factor				
Mask name	*Count*	*Sum*	*Average*	*Variance*
Fiberplast	2	0.198	0.099	0.003
Aqua variable perf	4	0.528	0.132	0.002
Aqua thick	3	0.406	0.135	0.002
Fiber variable perf	6	0.657	0.109	0.002
Embrace	3	0.208	0.069	0.0005
AccuPerf	3	0.215	0.072	0.0005
Aquaplast	4	0.245	0.061	0.00013

Table 19. The averaged medians pressure with the variance of the medians for all masks at the nose location.

ANOVA test result at nose location					
Source of Variation	*SS*	*df*	*MS*	*F*	*F critical*
Between Groups	0.019	6	0.003	2.126	2.661
Within Groups	0.027	18	0.0015	----------	----------
Total	0.047	24	----------	----------	----------

Table 20. The result of F test (ANOVA) at the nose location.

Table 20 showed that the F value is not greater than F critical, therefore the averaged median pressures for all masks are not significantly different among them. Thus, the Scheffe test are not needed to be applied at the nose location.

3.7.4. Averaged median pressure for all masks at the chin location

The following table will show the medians and the averaged medians for all masks at the chin location.

The median and the averaged median pressure [MPa] for all masks at the chin location							
Median	Aqua thick	Aqua variable perf	Fiberplast	Fiber variable perf	AccuPerf	Aquaplast	Embrace
1	0.149	0.152	0.058	0.087	0.069	0.046	0.038
2	0.194	0.128	0.043	0.049	0.071	0.054	0.039
3	0.199	0.074	0.059	0.050	0.048	0.049	--------
4	0.177	0.154	0.117	--------	0.053	0.051	--------
5	--------	0.131	--------	--------	0.043	0.018	--------
6	--------	0.092	--------	--------	0.056	--------	--------
7	--------	0.079	--------	--------	--------	--------	--------
Average	0.180	0.116	0.069	0.062	0.057	0.044	0.039
SD	0.022	0.033	0.032	0021	0.011	0.015	0.001

Table 21. The median and the averaged median pressure [MPa] for all masks at the chin location with the sample standard deviation.

The following tables will illustrate the F test (ANOVA) for the averaged median pressures of the masks at the chin location using Excel software.

Anova: Single Factor				
Mask name	*Count*	*Sum*	*Average*	*Variance*
Fiberplast	4	0.278	0.069	0.001
Aqua variable perf	7	0.812	0.116	0.001
Aqua thick	4	0.721	0.180	0.0005
Fiber variable perf	3	0.187	0.062	0.0005
Embrace	2	0.077	0.039	1.63027E-06
AccuPerf	6	0.342	0.057	0.0001
Aquaplast	5	0.220	0.044	0.0002

Table 22. The averaged median pressure with the variance of the median for all masks at the chin location.

ANOVA test result at the chin location					
Source of Variation	*SS*	*df*	*MS*	*F*	*F critical*
Between Groups	0.063	6	0.010	18.065	2.508
Within Groups	0.014	24	0.001	----------	-------
Total	0.077	30	----------	----------	-------

Table 23. The result of F test (ANOVA) at the chin location.

Since the F value is greater than F critical value at the chin location as shown in Table 28, therefore the averaged median pressures for all or some of the masks were significantly different. Hence, the Scheffe test was applied to find the averaged median pressures that were different from the others. The following table shows the results of the Scheffe test (F_S value) for all mask at the chin location using equation 15. The critical value (F') for the Scheffe test was 15.049.

Table of F_s values for comparison between masks						
Mask name	**Aqua variable perf**	**Aqua thick**	**Fiber variable perf**	**Embrace**	**AccuPerf**	**Aquaplast**
Fiberplast	9.495	42.267	0.153	2.184	0.650	2.467
Aqua variable perf	---------	18.088	10.449	16.043	19.423	25.989
Aqua thick	---------	---------	41.100	46.055	62.858	70.960
Fiber variable perf	---------	---------	---------	0.097	1.067	1.154
Embrace	---------	---------	---------	---------	0.865	0.073
AccuPerf	---------	---------	---------	---------	---------	0.775

Table 24. Table of Fs values for comparison between masks at the chin location.

Tables 24 reveals that the F_s value for Aqua thick was significantly different from the others and the F_s value for Aqua variable perf was significantly different with Embrace, AccuPerf and Aquaplast since the F_s test value of the compared mentioned masks is greater than the critical value F'. Whereas the other F_s value are smaller than the critical value which therefore referees to the averaged median pressure that was not significantly different.

Tables 14, 18 and 21 showed the highest averaged median pressure was due to Fiber variable perf at the forehead location (0.112 MPa) and Aqua thick at nose and chin (0.135 and 0.180 MPa, respectively). Whist, the lowest averaged median pressure was due to Aqua variable perf, Aquaplast and Embrace at the forehead, the nose and the chin locations, respectively (0.035, 0.061 and 0.039 MPa, respectively).

3.8. General discussion

These data suggest that masks begin to deform from the time that they are fabricated and continue for 48 hours, whereas one study found the internal shrinkage force of thermoplastic masks evaluated increased for only 24 hours (Bogdanov, 2003). The internal shrinkage force cannot be directly compared with these results since uniaxial shrinkage was not measured here. The CT scanning results, which measured the shrinkage after the mask was removed from a person's head that corresponded the amount of shrinkage from 0.12-192 hours presented in this work, showed that the variable perf masks exhibited a higher amount of shrinkage than the regular masks (Dovell et al., 2014a), while the amount shrinkage from 0.12-192 hours of variable perf masks were the least (Table 11). In this study, the AccuPerf mask shrank by 0.885%, while a previous study reported 6% (Rohrer). The following table shows a comparison between the previous work with the presented work.

The total amount of shrinkage in posterior/anterior direction from the previous work (Dovell et al., 2014a)				
Mask name	Forehead	Nose	Chin	Total shrinkage
Aquaplast	-----------------	1.01±0.03	1.23±0.10	0.7220
Fiberplast	-----------------	1.02±0.05	1.35±0.06	0.7226
Aqua variable perf	-----------------	1.05±0.06	1.01±0.09	0.7386
Fiber variable perf	-----------------	1.19±0.06	0.88±0.04	0.7298
The total amount of shrinkage in posterior/anterior direction from 0.12-192 hours presented in this work				
Aquaplast	1.532±0.026	1.830±0.030	1.544±0.027	-----------------
Fiberplast	0.814±0.023	1.473±0.025	1.406±0.025	-----------------
Aqua variable perf	0.8±0.024	1.125±0.020	1.084±0.022	-----------------
Fiber variable perf	0.71±0.035	0.882±0.028	0.827±0.031	-----------------

Table 25. comparison between the previous work (Dovell, et al., 2014b) with the presented work.

The percent of shrinkage from the previous work(Rohrer, n.d.)	
Mask's name	% of shrinkage
AccuPerf	6%
The percent of shrinkage from the presented work	
AccuPerf	0.810%

Table 26. Comparison between the previous work(Rohrer)with the presented work.

The 3mm spacer placed under the head rest of a patient during mask formations is an appropriate thickness to accommodate shrinkage since all masks exhibited an amount of shrinkage that is less than 3mm in posterior direction, but deform in inferior/superior and left/right directions. The overall effect of shrinkage results in a gap of 3mm that is present when the mask was remounted on the head phantom. Figure 29 illustrates the geometry used to confirm the gap deformations after mask shrinkage.

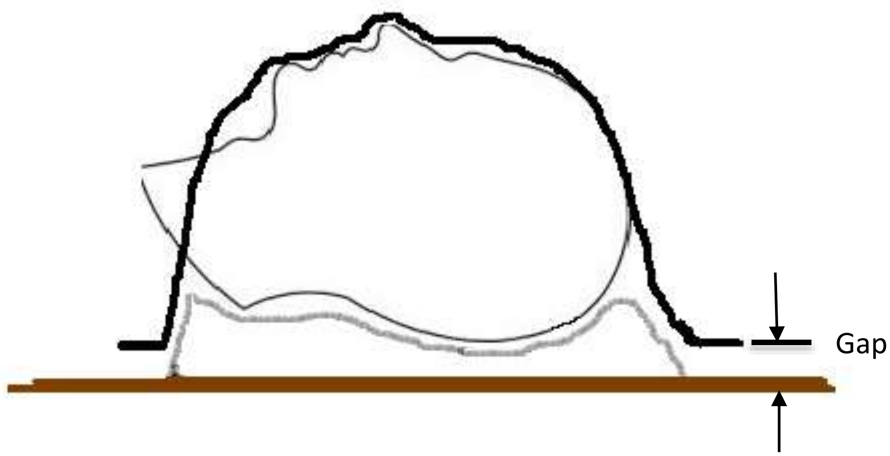

Figure 29. Illustration of the gap.

Fiber variable perf, which incorporates non-perforated strips, had the highest averaged median pressure at the forehead. Aqua thick, which has a uniform perforations, had the highest averaged median pressure at the nose and chin. This work is the first to measure pressure exerted by a thermoplastic mask.

4. CHAPTER 4: Conclusion

All masks started to deform by various amounts from the time of formation on the head phantom.

In terms of posterior translation, the two results obtained by the two different techniques, time-lapse photography and direct caliper measurement, did not agree for unknown reasons. An investigation of systematic error is needed to understand these discrepancies.

The greatest deformation in the superior/inferior direction was by the Embrace mask at forehead and nose areas(-1.069±0.017mm and -0.432±0.010mm, respectively), and by the Aqua thick mask at the chin area (0.970±0.016mm).

The relationship between the thicknesses of a mask and the amount of shrinkage is proportional, the thicker the mask is, the more shrinkage will occur. In the posterior direction, Aquaplast variable perforation masks shrink less than Fiberplast variable perforation, but Fiberplast masks are less deformed than Aquaplast masks. In superior/inferior direction, Fiberplast variable perforation masks are the least deformed.

The greatest averaged median pressure at forehead was due to Fiber variable perf (0.112 MPa). Whereas, at nose and chin, the greatest averaged median pressure was due to Aqua thick (0.135 and 0.180 MPa, respectively).

5. CHAPTER 5: Future work

It might be interesting to re-analyse the time-lapse photography images and measure pixel distance from the base-plate to the fiducial to try to understand the source of the discrepancy between the shrinkage measurement using the caliper technique and the shrinkage measurements using the time-lapse photography technique.

It would also be interesting to re-perform the pressure results using a various thicknesses of spacer for each mask so that the relative thickness that gives a constant pressure could be determined.

It would be interesting to study the effect of different thermal treatment on the amount of shrinkage.

All the measurements of the deformation obtained in this study were in posterior and superior/inferior directions, therefore measuring the amount of deformation in left/right direction would be a logical extension of this work.

References

Bluman, A. (2009). *Elementary statistics* (7th ed., p. 897). New York,: McGraw-Hill.

Bogdanov, B. (2003). ISOMETRIC CRYSTALLIZATION OF STRETCHED POLY (e - CAPROLACTONE) SHEETS FOR MEDICAL APPLICATIONS, *72*, 667–674.

Campbell, M. (2006). Statistical Distributions (e.g. Normal, Poisson, Binomial) and their uses. Retrieved from http://www.healthknowledge.org.uk/public-health-textbook/research-methods/1b-statistical-methods/statistical-distributions

Dovell, V., Bhutto, S., Doerwald-Munoz, L., Ostapiak, O. P., & Sawesky, G. O. P. . (2014a). Assessment of Comfort and Shrinkage in Four Styles of Thermoplastic Masks, *45*(2), 63–188.

Dovell, V., Bhutto, S., Doerwald-Munoz, L., Ostapiak, O. P., & Sawesky, G. O. P. . (2014b). Assessment of Comfort and Shrinkage in Four Styles of Thermoplastic Masks.

Fast Fourier Transform Calculator. (n.d.). Retrieved from http://www.random-science-tools.com/maths/FFT.htm

Ferreira, Tiago and Rasband, W. (2012). ImageJ User Guide. Retrieved from http://imagej.nih.gov/ij/docs/guide/user-guide.pdf

Fuji Prescale Film. (2001). Fuji Presc. Retrieved from http://www.spareonweb.com/tn_presc.htm

Fujifilm. (n.d.). Pressure measurement film prescale. Retrieved from http://www.fujifilm.com/products/prescale/prescalefilm/#overview

Fuss, M., Salter, B. J., Cheek, D., Sadeghi, A., Hevezi, J. M., & Herman, T. S. (2004). Repositioning accuracy of a commercially available thermoplastic mask system. *Radiotherapy and Oncology : Journal of the European Society for Therapeutic Radiology and Oncology*, *71*(3), 339–45. doi:10.1016/j.radonc.2004.03.003

Gilbeau, L., Octave-Prignot, M., Loncol, T., Renard, L., Scalliet, P., & Gregoire, V. (2001). Comparison of setup accuracy of three different thermoplastic masks for the treatment of brain and head and neck tumors. *Radiotherapy and Oncology : Journal of the European Society for Therapeutic Radiology and Oncology*, *58*(2), 155–62. Retrieved from http://www.ncbi.nlm.nih.gov/pubmed/11166866

ICRU 62. (1999).

Joergensen, D. (2012). digiCamControl. Retrieved from http://digicamcontrol.com/

Miller, M. B. (n.d.). Aperture, Shutter Speed, ISO, and Depth of Field. Retrieved from http://marlimillerphoto.com/camerabasics.pdf

Nikon. (2014). Nikon Digital SLR Camera D7000 Specifications. Retrieved from http://imaging.nikon.com/lineup/dslr/d7000/spec.htm

Q-fix. (2013). No Title. Retrieved from http://www.qfix.com/medical-professionals/brochures/QfixCatalog2013.pdf

Rasband, W. (n.d.). ImageJ 1.48v. National institutes of health, USA. Retrieved from http://imagej.nih.gov/ij

Rohrer, S. (n.d.). *shrinkage and thermoplastic* (p. 1). Retrieved from http://www.klaritymedical.com/Assets/Documents/TechDocs/Tech_Shrinkage_Eval_OSU_Klarity.pdf

Sensor Products Inc. (n.d.). Topaq® Pressure Analysis System. Retrieved from http://www.sensorprod.com/topaq.php

Sharp, L., Lewin, F., Johansson, H., Payne, D., Gerhardsson, A., & Rutqvist, L. E. (2005). Randomized trial on two types of thermoplastic masks for patient immobilization during radiation therapy for head-and-neck cancer. *International Journal of Radiation Oncology, Biology, Physics*, *61*(1), 250–6. doi:10.1016/j.ijrobp.2004.04.047

Sony. (n.d.). What is the relationship between aperture, shutter speed, and ISO? Retrieved from https://us.en.kb.sony.com/app/answers/detail/a_id/39650/~/what-is-the-relationship-between-aperture,-shutter-speed,-and-iso?

Sweeney, R. B. S., Bale, R. M. D., Vogele, M., Nevinny-Sticke, M., Bluhm, A. R. T. T., Auer, T. B. S., … Lukas, P. M. . (1998). REPOSITIONING ACCURACY: COMPARISON OF A NONINVASIVE HEAD HOLDER WITH THERMOPLASTIC MASK FOR FRACTIONATED RADIOTHERAPY AND A CASE REPORT, *41*(2), 475–483.

Thornton, A. J., Ten Haken, R., Gerhardsson, A., & Correll, M. (1991). Three-dimensional motion analysis of an improved head immobilization system for simulation, CT, MRI, and PET imaging, *20*(4), 224–8.

What Are Thermoplastics? (2007). Retrieved from http://www.scottstool.com/thermoplastic.htm

Zhang, M. (2012). A Great Graphic for Understanding How ISO, Aperture, and Shutter Speed Work. Retrieved from http://petapixel.com/2012/10/03/a-great-graphic-for-understanding-how-iso-aperture-and-shutter-speed-work/